Univerzita Karlova v Praze
Matematicko-fyzikální fakulta

BAKALÁŘSKÁ PRÁCE

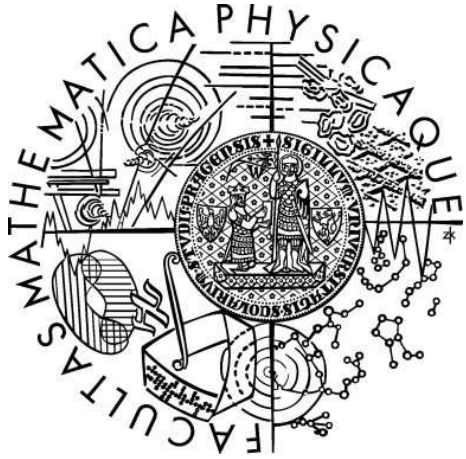

Tomáš Husek

Search for an Axion in OSQAR Experiment at CERN

Katedra fyziky nízkých teplot

Vedoucí bakalářské práce: prof. Ing. Miroslav Finger, DrSc.

Studijní program: Fyzika

Studijní obor: Obecná fyzika

Praha 2011

Charles University in Prague
Faculty of Mathematics and Physics

BACHELOR THESIS

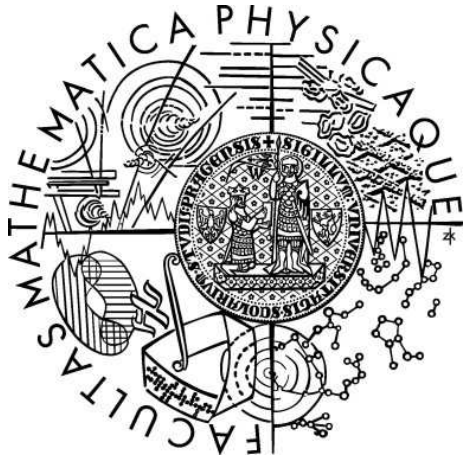

Tomáš Husek

Search for an Axion in OSQAR Experiment at CERN

Department of Low Temperature Physics

Supervisor of the bachelor th.: prof. Ing. Miroslav Finger, DrSc.

Study programme: Physics

Specialization: General Physics

Prague 2011

Poděkování

Na prvním místě bych chtěl poděkovat svému vedoucímu prof. Ing. Miroslavu Fingerovi, DrSc. za jeho podporu a možnost účastnit se experimentu OSQAR. Mé díky patří také Dr. Pierru Pugnatovi, který se stal mým plnohodnotným vedoucím přímo na měřeních v CERN a s nímž bylo velice zajímavé spolupracovat. Nesmím zapomenout na ostatní členy experimentu a své kolegy, jmenovitě pak na Ing. Karolínu Macúchovou, Ing. Miloslava Slunečku, Ing. Miroslava Krále, Ph.D. a Dr. Matthiase Schotta, kteří byli vždy nadosah a připraveni k všemožným diskuzím. Jsem také velice vděčný za pečlivé čtení, připomínky a trefné dotazy svého konzultanta RNDr. Ivana Procházky, CSc., jehož zkušenosti a vnější náhled mi byly velkým přínosem.

Během posledních optimalizačních měření, která proběhla v Praze u nás na fakultě na Katedře fyziky nízkých teplot, byla pomoc mnoha lidí naprosto zásadní. Chtěl bych poděkovat prof. RNDr. Josefu Štěpánkovi, CSc. z Oddělení fyziky biomolekul, že souhlasil se zapůjčením nevyužitého CCD detektoru a doc. Ing. Petru Prausovi, CSc., který díky svým zkušenostem nabitým dřívější prací s ním byl vždy velmi ochotný odpovídat na mé otázky ohledně hardwarových parametrů. Ing. Miloš Pfeffer, CSc. je člověkem dobré vůle a byl vždy trpělivý ohledně věcí spojených s použitím vhodného počítače a otázek funkčnosti a mé díky patří i jemu. Konečně, bylo nutno nalézt volné místo v nízkoteplotní laboratoři a zařídit vakuové vývěvy a tekutý dusík. Díky Mgr. Vojtěchu Chlanovi, Ph.D. proběhlo vše velmi hladce a bez problémů, protože vše, co jsem potřeboval, bylo ihned zařízeno.

Nakonec bych se chtěl omluvit, a to svým nejbližším, že jsem trávil tak mnoho času prací místo toho, abych byl s nimi, a také těm, na které jsem eventuálně nedopatřením zapoměnl, ač by si mé díky zasloužili.

Acknowledgments

On the first place I would like to thank to my supervisor prof. Ing. Miroslav Finger, DrSc. for his support and for the opportunity of participating in OSQAR experiment. My gratitudes go also to Dr. Pierre Pugnat, who supervised the measurements directly at CERN and with whom it was very interesting to work. I can't forget other members of OSQAR and my colleges, namely then Ing. Karolína Macúchová, Ing. Miloslav Slunečka, Ing. Miroslav Král, Ph.D. and Dr. Matthias Schott, who were always near and ready for various discussions. I am also very grateful for attentive reading, advices and ingenious questions of my consultant RNDr. Ivan Procházka, CSc., whose experiences and outer point of view were really conducive.

During the last optimizing measurements, which took place in Prague at the Department of Low Temperature Physics at our faculty, the help of many people was quite essential. I would like to thank to prof. RNDr. Josef Štěpánek, CSc. from Division of Biomolecular Physics, that he agreed to borrow us presently unused CCD detector, and to doc. Ing. Petr Praus, CSc., who had experiences from working with this camera and was always very kind to answer my questions about hardware settings and parameters. Ing. Miloš Pfeffer, CSc. is a man of a good will and was very patient about things connected with available computer stuff and its functioning and my thanks belong also to him. Finally, some spare work place in the laboratory of low temperatures was needed to be found, vacuum pumps and liquid nitrogen used. It was thanks to Mgr. Vojtěch Chlan, Ph.D., that everything went very smooth and without any problems, because all my needs were immediately solved.

I have to also apologize to people very close and related to me, that I did spend so much time working instead being with them, and also to those, who I had accidentally forgotten though they deserved my thanks too.

Prohlašuji, že jsem tuto bakalářskou práci vypracoval samostatně a výhradně s použitím citovaných pramenů, literatury a dalších odborných zdrojů.

Beru na vědomí, že se na moji práci vztahují práva a povinnosti vyplývající ze zákona č. 121/2000 Sb., autorského zákona v platném znění, zejména skutečnost, že Univerzita Karlova v Praze má právo na uzavření licenční smlouvy o užití této práce jako školního díla podle §60 odst. 1 autorského zákona.

I declare that I carried out this bachelor thesis independently, and only with the cited sources, literature and other professional sources.

I understand that my work relates to the rights and obligations under the Act No. 121/2000 Coll., the Copyright Act, as amended, in particular the fact that the Charles University in Prague has the right to conclude a license agreement on the use of this work as a school work pursuant to Section 60 paragraph 1 of the Copyright Act.

V Praze dne / In Prague, date ..... 2011 Podpis autora / Signature

.....

Název práce: Pátrání po axionech na experimentu OSQAR v CERN
Autor: Tomáš Husek
Katedra (ústav): Katedra fyziky nízkých teplot
Vedoucí bakalářské práce: prof. Ing. Miroslav Finger, DrSc.
e-mail vedoucího: Miroslav.Finger@cern.ch

Abstrakt: V předložené práci je představen experiment OSQAR v CERN. Cílem tohoto spíše malého experimentu je pátrání po hypotetické částici zvané axion, která by měla hrát důležitou roli v moderních fyzikálních teoriích. Je důležité zmínit, že celkové experimentální uspořádání stejně jako jednotlivá zařízení jsou ve stadiu vývoje a kalibrace a měřící režimy jsou stále optimalizovány. Proto je diskutována požadovaná funkčnost a spolehlivost v současnosti používaného vybavení spolu s řadou možných měřících postupů. Přiloženy jsou také předběžné výsledky, simulace a odhady na citlivost stávajícího experimentálního uspořádání.

Klíčová slova: axion, supravodivý dipól, laserové světlo

Title: Search for an Axion in OSQAR Experiment at CERN
Author: Tomáš Husek
Department: Department of Low Temperature Physics
Supervisor: prof. Ing. Miroslav Finger, DrSc.
Supervisor's e-mail address: Miroslav.Finger@cern.ch

Abstract: In the present work, OSQAR experiment at CERN is being introduced. The goal of this rather small experiment is a search for a hypothetical particle called axion, which could play an important role in modern physical theories. It is necessary to say, that the experimental setup as well as particular devices are still being developed or calibrated and measurement modes optimized. That is why desired functionality and reliability of the presently used equipment with a variety of different operating procedures are discussed. Preliminary results, simulations and estimation of sensitivity limitations of the current setup are also presented.

Keywords: axion, superconducting dipole, laser light

Contents

To my parents

Introduction

When looking for new particles, not only TeV colliders such as LHC (Large Hadron Collider) are needed to be built. Many extensions of the Standard Model, in particular those based on supergravity or superstrings, predict not only massive particles like WIMPs (Weakly Interacting Massive Particles), but also WISPs (Weakly Interacting Sub-eV Particles), such as the axion. The detection of the latter mentioned particles should be possible in low energy experiments based for example on lasers, cavities, strong electromagnetic fields etc. The OSQAR experiment [1, 2, 3, 4] emerges low energy frontier of particle/astroparticle physics.

Axions are hypothetical elementary particles promising to solve some fundamental problems in modern physics (strong CP problem, dark matter etc.). According to the theoretical models it is expected, that axions are very weakly interacting particles. In order to experimentally detect them, the use of colorful and inspired techniques becomes mandatory [5]. During last 30 years, various experimental approaches were developed [6] and many of them use the Primakoff effect (the photon-axion conversion in the presence of the strong electromagnetic field). Though number of experiments attempted to detect this hypothetical particle, there were still no positive results published.

The OSQAR experiment uses strong magnetic fields (provided by LHC dipoles) combined simultaneously with the powerful laser beam in two distinct experiments (the photon regeneration and ultra-fine magnetic birefringence of the vacuum) to prove experimentally the existence of axions or disconfirm the hypotheses in specific mass/coupling regions. Furthermore, also other particles such as light scalars on paraphotons could arise from the measurements depending on the setup of the experiment.

In OSQAR Collaboration participate 11 institutions from 4 countries. At present, the experiment is in the state of preparation. The experimental setup as well as particular devices are still being developed or calibrated and measurement modes optimized. Concerning the specific characteristics of the setup, the great advantage lies in the use of two LHC dipoles, each of which produces very homogenous and strong magnetic field 9 T on an impressive length 14.3 m. The laser beam going through this field is then of the power up to 20 W (present state).

In this work, we get from historical and theoretical background through the presentation of the setup of OSQAR experiment and data acquisition strategy to the innovative change proposals. The properties of particular parts of the experimental setup (especially the laser and CCD detector) are being discussed, calibration measurements done and improvements proposed. These are the important steps to go further in the search, to increase the sensitivity to explore wider range of possible axion properties.

Chapter 1

Basic facts

1.1 OSQAR collaboration

The acronym OSQAR stands for quite a long term: Optical Search of QED vacuum magnetic birefringence, Axion and photon Regeneration. In OSQAR Collaboration participate 11 institutions (including Faculty of Mathematics and Physics at Charles University in Prague) from 4 countries (Czech Republic, France, Poland and Schwitzerland). It was officially approved in 2007 and at present it is in the state of preparation.

The experimental setup takes place in the LHC (Large Hadron Collider) test hall (SM18) at CERN (European Organization for Nuclear Research, Geneve, Schwitzerland), where two spare LHC dipole magnets are for this purpose accessible together with all necessary related infrastructure for cooling them down to low temperatures (Fig. 1.1).

1.2 Axion historical background

Axion is a hypothetical elementary neutral spin-zero particle, more precisely a light pseudo-Nambu-Goldstone boson [7, 8]. Its history started in 1977, when Roberto Peccei and Helen Quinn proposed their (still the most well-known and plausible) solution to the strong CP problem [9]. This problem is based on the fact, that there are terms in the QCD (Quantum Chromodynamics) Lagrangian which are able to break the CP-symmetry, but from experiments (such as neutron electric dipole moment measurements [10]) there is no indication of any CP violation in the QCD sector (compared for example to the electroweak theory). With the Peccei-Quinn symmetry, a light and weakly interacting particle is associated that was named by Frank Wilczek based on experience from day-to-day life: *I named them after a laundry detergent, since they clean up a problem with an axial current* (Frank Wilczek, Nobel lecture 2004) ([8] preface, [11]). The existence of our mysterious particle was also independently predicted by Steven Weinberg [7].

In addition to fundamental problems in QCD, axions are also hot candidates for the so called cold dark matter (dark for that it cannot be observed by its electromagnetic radiation, and cold because its constituent particles move slowly) and similar particles are naturally presented in the string theory too.

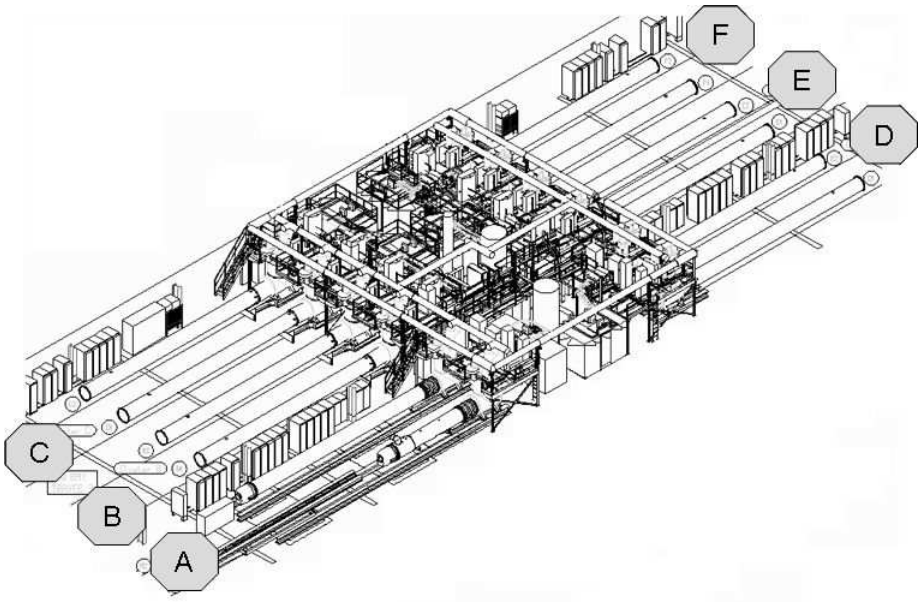

Figure 1.1: Layout of the LHC superconducting magnet test plant consisting of 12 test benches grouped in 6 clusters (A to F) in the SM18 hall. The benches B1 and E1 (in the tight neighbourhood of sectors A and D) are provided for OSQAR.
source: <http://cdsweb.cern.ch/record/1072483/files/spsc-2007-039.pdf>

1.3 Experimental verification of the existence of the axion

There are in principle two ways, how to verify the existence of axions in a purely laboratory self-dependent experiment, in both cases using the laser induced measurements. Namely we talk about the "light shining through a wall" (or the photon regeneration) experiment and tests probing the magneto-optical properties of the vacuum (referring to Vacuum Magnetic Birefringence or VMB).

The first (rather direct) method will be discussed later, because it is at present the leading goal of the OSQAR experiment. The later mentioned (rather indirect) method based on the measuring of VMB has its roots quite deep in the past (in 1936) since this effect was predicted by Euler, Heisenberg and Weisskopf [5]. According to QED (Quantum Electrodynamics), the vacuum behaves as an optically active medium in the presence of an external magnetic field, what can be tested experimentally with a linearly polarized laser beam propagating perpendicularly to the field direction. In this way, the linear polarization of the laser beam should change to elliptical. But contributions to the VMB could also arise from the existence of light scalar or pseudoscalar particles like axions that couple to two photons and this would manifest itself as a sizable deviation from the initial pure QED prediction. But this very fine effect is difficult to measure and represents quite a great challenge for optical measurement techniques.

Effects of the magnetic field on the vacuum causing the rotation of the polarization of the laser light was tested in PVLAS (Polarizzazione del Vuoto con LASer) experiment in Legnaro National Laboratory of National Institute of Nuclear Physics near Padova, Italy [12]. Although it was for the first time, when a positive result regarding the existence of axions was measured, it was soon disclaimed. Other experiments concerning the axion problem are for example ALPS (Any Light Particle Search) at DESY, Germany [13], which is now the competition for OSQAR or the BMV project (Birefringence Magnetique du Vide), France [14].

1.4 Experimental setup

The setup of the OSQAR experiment at present is quite simple (schematically shown in Fig. 1.2). Everything starts with a high power laser (details in section 4.1), whose beam is with the help of mirrors properly directed into the entrance of the LHC dipole magnet (details in section 4.3). Here the photons of the laser beam interact with the virtual photons of the magnetic field, which should lead in a conversion (Primakoff effect) to an axion (similar to quantum oscillations of neutrinos [1]). Going through the whole magnet the primary laser beam is being stopped by the usual brick just after it leaves the dipole on the other side. Axions, that could arise from the photon-photon interaction, are very weakly interacting with the normal matter, hence it is easy for them to propagate behind the brick into the second superconducting magnet of the same type as the first one. Here the reverse conversion process takes place. In the positive case, photons are generated in the magnetic field and through the focusing lens strike upon the CCD (charge-coupled device) detector (details in section 4.2) at the end of the dipole, the last part of the setup, where they are registered.

Using a similar principle, another experiment called CAST (CERN Axion Solar Telescope) is running in CERN [15]. But in this case, not laser induced axions but in the sun produced particles should be converted back to photons in the old LHC dipole prototype magnetic field to be detected in the X-ray region.

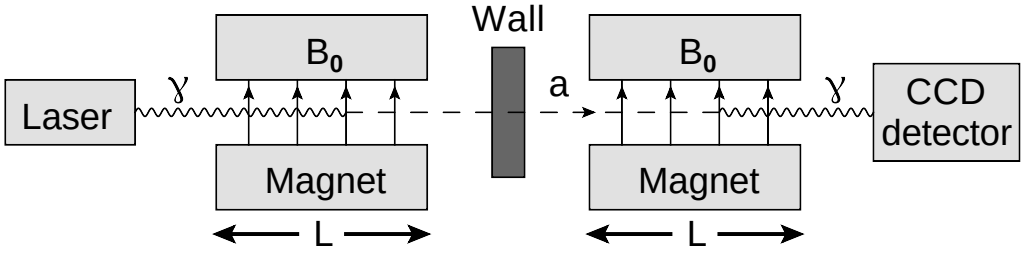

Figure 1.2: Basic experimental setup for a photon regeneration experiment

Chapter 2

Derivation of conversion probability

The light neutral pseudoscalar ϕ_p couples to two photons through fermions via the triangle anomaly [6]. To show briefly the basic calculation of a photon to axion conversion probability we consider the Lagrangian density $\mathcal{L}$ of the form

$$\mathcal{L} = -\frac{1}{4\mu_0} F_{\mu\nu} F^{\mu\nu} + \frac{1}{2\hbar c}\left[\partial_\mu \phi_p \partial^\mu \phi_p - \left(\frac{m_p c}{\hbar}\right)^2 \phi_p^2\right] + \frac{1}{4\mu_0} g \phi_p F_{\mu\nu} \tilde{F}^{\mu\nu}\,, \qquad (2.1)$$

where m_p is the pseudoscalar mass, g is a coupling constant and $F_{\mu\nu}$ and $\tilde{F}^{\mu\nu}$ are electromagnetic field tensor and its dual tensor respectively defined as (while A_μ being electromagnetic 4-potential)

$$F_{\mu\nu} = \partial_\mu A_\nu - \partial_\nu A_\mu \qquad \tilde{F}^{\mu\nu} = \frac{1}{2}\epsilon^{\mu\nu\kappa\lambda} F_{\kappa\lambda}\,. \qquad (2.2)$$

Obviously, the first term in the Lagrangian (2.1) describes the electromagnetic field, the second is leading to the well-known Klein-Gordon equation for the pseudoscalar ϕ_p and the third one is the interaction term.

Euler-Lagrange equation of motion for a field ϕ is

$$\partial_\mu \left(\frac{\partial \mathcal{L}}{\partial(\partial_\mu \phi)}\right) = \frac{\partial \mathcal{L}}{\partial \phi}\,. \qquad (2.3)$$

If we use this formula for both ϕ_p and A_ν (considering a static magnetic filed and real photons [16]), we get

$$\frac{\mu_0}{\hbar}\left[\partial_\mu \partial^\mu + \left(\frac{m_p c}{\hbar}\right)^2\right]\phi_p = g\mathbf{E}\cdot\mathbf{B}$$

$$\partial_\mu \left[F^{\nu\mu} + g(\phi_p \tilde{F}^{\mu\nu})\right] = 0\,. \qquad (2.4)$$

Now we should introduce the notation used in the following text. The Energy of the initial photon (E_γ) as of the pseudoscalar (E_p) is

$$E_\gamma = E_p = \hbar\omega \qquad (2.5)$$

and their momenta are then

$$p_\gamma = \hbar k_\gamma = \frac{E_\gamma}{c} = \frac{\hbar\omega}{c} \qquad p_p = \hbar k_p = \frac{1}{c}\sqrt{E_p^2 - m_p^2 c^4} = \sqrt{\left(\frac{\hbar\omega}{c}\right)^2 - m_p^2 c^2}\,. \qquad (2.6)$$

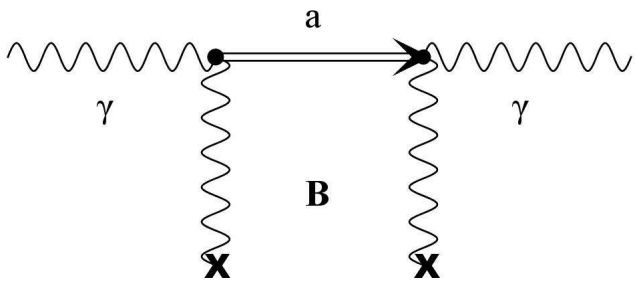

Figure 2.1: Feynman diagram for an axion exchange

In [6], the solution of equations (2.4) is written in the form (note that rationalized natural units are used, in which we put $\hbar$=c=1)

$$\phi_p^{(\pm)}(\mathbf{r},t) = e^{-i\omega t}\int \frac{1}{4\pi}\frac{e^{\pm ik_p|\mathbf{r}-\mathbf{r}'|}}{|\mathbf{r}-\mathbf{r}'|} g\mathbf{E}(\mathbf{r}')\cdot\mathbf{B}(\mathbf{r}')\mathrm{d}^3r' \tag{2.7}$$

If we consider the magnetic field

$$\mathbf{B}(\mathbf{r}) = \hat{\mathbf{x}}B(z) \tag{2.8}$$

and the polarization of the laser beam

$$\mathbf{E}(\mathbf{r},t) = \mathbf{E}(\mathbf{r})e^{-i\omega t} = \hat{\mathbf{x}}E_0 e^{ik_\gamma(z-ct)} \Longrightarrow \mathbf{B} \parallel \mathbf{E}\,, \tag{2.9}$$

we can write the solution (2.7) in the form

$$\phi_p^{(+)}(\mathbf{r},t) = \frac{iE_0}{2k_p} g\left(\int B(z)\mathrm{d}z\right) F(\omega-k_p)e^{i(k_pz-\omega t)}\,, \tag{2.10}$$

what leads to the probability $\Pi_{\gamma a}$ of a photon to axion conversion ($\gamma\gamma \leftrightarrow a$, see Fig. 2.1) in an external static homogeneous magnetic field $B(z)$=B_0 acting on the length L measured in the direction of the laser beam propagation (parallel to $\hat{\mathbf{z}}$)

$$\Pi_{\gamma a} = \left(\frac{\omega}{k_p}\right)\left(\frac{gB_0L}{2}\right)^2 |F(\omega-k_p)|^2\,, \tag{2.11}$$

where $F(q)$ is a form factor for the magnetic region

$$F(q) = \frac{\int B(z)e^{-iqz}\mathrm{d}z}{\int B(z)\mathrm{d}z}\,, \tag{2.12}$$

which in our case has the form

$$|F(q)|^2 = \frac{1}{L^2}\left|\int_0^L e^{-iqz}\mathrm{d}z\right|^2 = \mathrm{sinc}^2\left(\frac{qL}{2}\right)\,. \tag{2.13}$$

According to more precise and better documented way in [17], the following result is obtained (using our notation)

$$|\phi^{(1)}_{\mathrm{Trans}}(z,t)|^2 = \frac{(gB_0)^2}{m_p^4}\left(\frac{\omega^2}{k_p^2}\right)(\omega+k_p)^2\sin^2\left[\frac{L}{2}(\omega-k_p)\right], \tag{2.14}$$

which is in accordance to (2.11), when we consider that

$$\frac{(\omega+k_p)^2}{m_p^4} = \frac{(\omega^2-k_p^2)^2}{(\omega-k_p)^2 m_p^4} = \frac{1}{(\omega-k_p)^2}. \tag{2.15}$$

For axion to photon conversion we would get

$$|a^{(1)}_{\mathrm{Trans}}(z,t)|^2 = \frac{(gB_0)^2}{m_p^4}(\omega+k_p)^2\sin^2\left[\frac{L}{2}(\omega-k_p)\right]. \tag{2.16}$$

To sum it up, we could write for both processes

$$\Pi_{\gamma a} = \left(\frac{gB_0L\omega}{2k_p}\right)^2 \mathrm{sinc}^2\left(\frac{qL}{2}\right) \qquad \Pi_{a\gamma} = \left(\frac{gB_0L}{2}\right)^2 \mathrm{sinc}^2\left(\frac{qL}{2}\right). \tag{2.17}$$

Consider then the situation when $m_p \ll \omega$, then $\omega/k_p \simeq 1$ and

$$q = \omega - k_p = \omega - \omega\sqrt{1-\frac{m_p^2}{\omega^2}} \simeq \omega\left[1-\left(1-\frac{m_p^2}{2\omega^2}\right)\right] = \frac{m_p^2}{2\omega}. \tag{2.18}$$

In case that $m_p^2L/4\omega$ is also small, then $\mathrm{sinc}^2(qL/2) \simeq 1$ and finally we have [6]

$$\Pi_{\gamma a} \simeq \Pi_{a\gamma} \simeq \left(\frac{gB_0L}{2}\right)^2. \tag{2.19}$$

Otherwise, when the conversion process takes place in the medium of refractive index $n_r = \sqrt{\epsilon}$, probability introduced in (2.11) (together with (2.13)) is modified [1, 18] into

$$\Pi_{\gamma a} = \frac{\omega}{n_r k_p}\left(\frac{gB_0L}{2}\right)^2 \mathrm{sinc}^2\left(\frac{qL}{2}\right). \tag{2.20}$$

Considering the appropriate change in the photon momentum, one have to choose between two interpretations. A solution of the well-known Abraham-Minkowski controversy was recently shown [19]. Due to the character of our experiment, kinetic momentum (Abraham form) is used, i.e. $k_\gamma = \omega/n_r$. We have then for momentum transfer

$$q = \frac{\omega}{n_r} - k_p = \omega\left(\frac{1}{n_r} - \sqrt{1-\frac{m_p^2}{\omega^2}}\right). \tag{2.21}$$

The maximum of conversion probability (2.20) corresponds to the limit $q \to 0$, hence the optimal refractive index would be (again we consider $m_p \ll \omega$)

$$n_r = \left(\frac{1}{\sqrt{1-\frac{m_p^2}{\omega^2}}}\right) \simeq \left(1+\frac{m_p^2}{2\omega^2}\right). \tag{2.22}$$

Then we have $n_r \simeq 1$. These conditions are obtainable when the air of suitable pressure is used as the medium.

Leaving the axions for a while, it can be noted that if the polarization of the laser beam was set to be perpendicular to the magnetic field

$$\mathbf{E}(\mathbf{r},t) = \mathbf{E}(\mathbf{r})e^{-i\omega t} = \hat{\mathbf{y}}E_0 e^{ik_\gamma(z-ct)} \Longrightarrow \mathbf{B} \perp \mathbf{E}\,, \tag{2.23}$$

the same experimental setup should be sensitive for light scalar particles. For a scalar field ϕ_s [1] the Lagrangian density (2.1) would change into

$$\mathcal{L}_s = -\frac{1}{4\mu_0}F_{\mu\nu}F^{\mu\nu} + \frac{1}{2\hbar c}\left[\partial_\mu\phi_s\partial^\mu\phi_s - \left(\frac{m_s c}{\hbar}\right)^2\phi_s^2\right] + \frac{1}{4\mu_0}g\phi_s F_{\mu\nu}F^{\mu\nu}\,. \tag{2.24}$$

Then the equations of motion (2.4) can be rewritten in the form

$$\frac{2\mu_0 c}{\hbar}\left[\partial_\mu\partial^\mu + \left(\frac{m_s c}{\hbar}\right)^2\right]\phi_s = g\left(c^2\mathbf{B}^2 - \mathbf{E}^2\right)$$

$$\partial_\mu\left[F^{\nu\mu} + g(\phi_s F^{\mu\nu})\right] = 0\,. \tag{2.25}$$

The photon regeneration experiment can be also performed, when no magnetic field is applied (i.e. $\mathbf{B}$=0). In this case a search for paraphotons γ_p is done. The oscillations should occur between the noninteracting massive photon (or paraphoton) and the massless interacting one with the probability

$$\Pi_{\gamma\gamma_p} \simeq \left(\frac{m_{\gamma_p}^2 L}{4\omega}\right)^2 \sin\theta\,, \tag{2.26}$$

where θ is the mixing angle and m_{γ_p} is the paraphoton mass [3].

Chapter 3

Axion search

3.1 Introduction

The search for axions using a typical setting of the photon regeneration experiment still remains the main aim of the OSQAR experiment. In this case, the formula (2.19) is crucial (note that rationalized natural units are used, in which we put $\hbar$=c=1)

$$\Pi \simeq \frac{1}{4}(gB_0L)^2, \tag{3.1}$$

where Π is a probability (i.e. a dimensionless quantity) of a photon to axion conversion (and vice versa) in an external static homogeneous magnetic field B_0 acting along the length L measured in the direction of the laser beam propagation and g is a coupling constant.

At the OSQAR experiment there is one substantial advantage in a possibility of using two LHC dipole magnets to produce a strong homogeneous magnetic field (B_0=9 T) on a quite impressive length (L=14.3 m) in the long term (details in section 4.3). Thus in (3.1) we have then only one unknown parameter g and the rest is given by the setup of the experiment.

If we would like to estimate an expected number of photons detected by the detector per unit of time n, we should calculate the number of photon emitted by the laser per one second and multiply it with the conversion probabilities introduced above. We can detect photons only after their at least double conversion due to the effects of the magnetic field. The final formula is then (using SI units) given by

$$n = \frac{P\lambda}{hc}\Pi^2\eta, \tag{3.2}$$

where P is the power of the laser, λ is the wavelength of the laser light, h=$2\pi\hbar$ is the Planck constant and η is the overall efficiency of the experimental setup (including detector sensitivity, reflection losses etc.). These parameters (related to the laser and detector) can all be altered.

3.2 Data acquisition

The whole experiment is deeply dependent on the superconducting magnets. This is tightly connected with cooling them down to 1.9 K. During the summer 2010 we had an opportunity to make some measurements.

In general, the procedure of data acquisition is as follows. At first it is necessary to turn on the magnetic field. The linearly polarized photon beam coming from the laser tube (the direction of the polarization is vertical, parallel to the magnetic field) is then properly aligned through the pipes in the pair of superconducting dipoles and the focusing lens into the detector so a round undeformed spot on the CCD chip covering should be visible. After that, the brick is put between the magnets and the parts around the detector are tightly covered to prevent photons from the surroundings to make an artificial signal. This, for the light isolated space, we call the dark chamber (the term is used later). Then only the power of the laser is set to the maximum and the measurement could be started. In this setup, pseudoscalars should be generated (2.7). All can be repeated with the perpendicular polarization of the beam with respect to the magnetic field orientation while light scalar particles are generated. After this part is finished, the laser should be turned off and the background measured. The last step is to check, if the alignment of the laser remained stationary. If everything is all right, the data can be used for further treatment. Detailed informations about conditions which could effect the measurements are written into the logbook.

It must be mentioned that during the last run (summer 2010) the procedure was not obeyed ideally according to previous description. The first priority was laid on the measurements with the laser beam linearly polarized perpendicular to the magnetic field (half-wave plate at 91°) and magnetic field switched on (i.e. not pseudoscalar but scalar particles production mode). The background was measured after the possibility of the cooling of the magnets ran out and the beam alignment check was made even later. Due to problems with the CCD detector no serious data with another beam polarization were acquired. Nevertheless, obtained data could be still used for the testing of functionality and for the optimization of the whole experimental setup.

3.3 Data treatment

The detector service software (details in section 4.2) generates files in SPE format containing predefined number of frames of an equal exposure time, which must be sorted very carefully (because of cosmic rays and noise issues, which will be discussed later). An example of the frame (i.e. single position spectrum measurement or some people could compare it to the camera shot) we worked with is in Fig. A.1, where also effects of a simple cosmic ray filtering are shown. In fact, in this case we use the term frame for the result of the hardware summation of all rows of the CCD chip (which is 2-dimensional) right after one measurement of exposure time ϵ is performed.

The files are at the beginning converted into more universal format thanks to our friend Vladimir Jary and his *spe-tools* solution [20]. The strategy of the data treatment is more or less simple. All the used frames are at first filtered from the cosmic rays (or cosmics, Fig. A.1, details in section 4.2). Then the signal (laser

ON) and background (laser OFF) frames are separately summed together and in the end subtracted from each other. If we plot the result as a curve, we should see in positive case a shape of the original laser beam growing up from the noise. After the simulation was done (see chapter 5), it does not seem to be necessary to make the final subtraction to get the result.

Final plots of the last measurements are shown in Fig. A.2, A.3 and A.4. You can find the file names and numbers of the used frames in the key of the plot. The summation of the signal frames is denoted by the line with plus sign on the position of each value point (-+-). The background one is then the curve with x sign (-x-). The intensity scale for two previously described lines is on the left vertical axis. Total integration time for each summation is written in the heading of the figure. Signal and background curves both consist of the same number of frames. The bottom curve is always the subtraction of the summation curves (signal–background) with the scale axis on the right.

3.4 Discussions

From the plots (Fig. A.2, A.3 and A.4) it is obvious, that in general, we did not find any clear proof for an existence of particles of our interest. But we can use the results also as the guide for future measurements. It is really important to choose the right exposure time. There are two main factors, which we must take into account: cosmics and electronic noise.

Although it is possible to avoid the cosmic rays to intrude into the measurements and to filter them in the end from the spectra, we cannot get rid of the noise. When the shutter (placed right before the chip) is opened for a very short time, not many of the coming photons can be recorded compared to the random noise. We can see the example in the data taken. From the 5 min expositions summed together (Fig. A.4) we can see, that our dark chamber was not ideal. Some photons were still able to go inside and make a noticeably change in the shape of a presumed straight line. Apparently the exposure time of 30 s (Fig. A.2) is not the right choice, because much of the parasitic signal (the background dark chamber conditions were the same) is hidden in the noise. But it is important that the level of the noise was in this case (30 s) for some reason (e.g. cooling) a little bit higher (see chapter 5) than in the long term measurements previously presented (5 min). Therefore this cannot serve as a proof although the common sense prefers the longer exposure time.

On the other hand, if the exposure time is too long, many of the cosmics are detected during one measurement and the forest of high sharp peaks appears. Afterwards these are filtered (details in section 4.2), at the same time it can be also dropped out a real photon signal, which could have been conversed from an axion. This way we would loose the useful information. But it seems that 5 min long exposition (Fig. A.4) is still acceptable.

Much more important than the noise, while getting to longer expositions, is the rate of cosmics. In fact, the best solution is to find as long exposure time as possible until this rate is too disturbing. It is more or less a sense issue.

3.5 Bending of the laser beam

Besides the main experiment we had an interesting result in another test. A very fine effect of the magnetic field on the direction of the laser beam was observed. The beam profile (50 frames) was measured during the time when the magnetic field was switched off. Then it was turned on and the measurements were done again. After the way through two strong LHC magnets (details in section 4.3) the position spectrum moved a little perpendicularly to the direction of the magnetic field, as shown in Fig. A.5. All the spectra were divided by their height and then summed together (with and without the field separately). Then the subtraction of these two final curves was made and put together with them into the plot.

From every single frame an expected position of the maximum was calculated (first moment method) and put into the plot to make a check. You can see the result in Fig. A.6. The curves are more or less one above each other, which means that we definitely have some discovery. Originally for all the spectra Gaussian fits were made (least squares method) and from the calculated parameters 5-sigma criterion was examined. The shift was in average 0.61 pixel with standard error 0.063. Their ratio is then nearly 10.

There still remains the question, what is the reason for this observation. If a photon had had a charge, most probably there should have been another one with an opposite charge too. But the spectrum moved, not widened (checked with the second central moment calculation). Although very high vacuum (typically 10^{-7} mbar) was present in the tube where magnetic field was applied, still some molecules remain there. That is why we believe the residual gases have something to do with it.

All usable measurements made up to now were done in February 2010. From the time we have a new laser (details in section 4.1), we are not able to continue in probing our assumptions, because the stability of the beam is not sufficient anymore. In the future, we would like to do some further measurements to prove or disconfirm our hypotheses. Also the time dependence (or relaxation time) of the effect should be checked.

In the end, limits of the sensitivity of the photon charge measurement (if there was any) could be established. We can imagine, that photon possesses a charge q. In that case, we could calculate a horizontal shift of the laser beam after it passes through the both LHC dipoles. Every charged particle of mass m moving in the magnetic field B with a velocity v is affected by the Lorentz force. The radius r of this (in our simple case) circular motion can be easily obtained from the equality with the centripetal force, hence using (2.6) in case of the photon we have

$$r = \frac{mv}{qB} = \frac{\hbar\omega}{qcB} = \frac{2\pi\hbar}{q\lambda B}\,. \tag{3.3}$$

The deviation of this curved trajectory from the straight line after passing through the first magnetic field region acting along the length L would be

$$\Delta x_1 = r - \sqrt{r^2 - L^2} \equiv r - s\,. \tag{3.4}$$

Then there is a gap of the length D between the dipoles, where the particle would move along the straight line. Supposing there was not any magnetic field in the second dipole, the overall deviation obtained in this middle region would be

$$\Delta x_2 = (D + L)\tan(\alpha)\,, \tag{3.5}$$

where $\sin(\alpha)=L/r$. Turning on the field, the last contribution (a little simplified, because the precise term is too ugly and in the end the difference has no serious effect) is

$$\Delta x_3 = \frac{1}{\cos(\alpha)}\left(r - \sqrt{r^2 - \left(\frac{L}{\cos(\alpha)}\right)^2}\right)\,. \tag{3.6}$$

The total deviation observed by the camera would be then

$$\Delta x = \sum_{i=1}^{3}\Delta x_i = r - s + \frac{L(D+L)}{s} + \frac{r^2}{s}\left(1 - \sqrt{1 - \left(\frac{L}{s}\right)^2}\right) \simeq$$

$$\simeq r - s + \frac{L(D+L)}{s} + \frac{r^2}{2s}\left(\frac{L}{s}\right)^2\,. \tag{3.7}$$

For D=10 m and considering that the available spatial resolution of the current CCD chip depends on the pixel size (which is about 25 μm) we obtain, that we are able to detect a deviation of the laser beam caused by the photon of a charge down to 10^{-35} C, what is approximately $6\times10^{-17}e$ and incomparable with present bounds of about $10^{-32}e$ [21].

This way it was proved, that observed phenomenon, which was discussed earlier, should not be explained by anything connected with a photon charge.

Chapter 4

Parameters of devices used (Summer 2010)

4.1 Laser

During the run in February 2010, the 20 W argon ion laser from Spectra Physics was used. We were able to have stable beam at 17 W. Unfortunately the laser stopped to function and it was necessary to look for a new one. This is what we got:

Manufacturer: Coherent
Type: INNOVA 400 Series Ion Laser
MODEL NO.: I-400
SERIAL NO.: 93200921
MFG. DATE: 9305

Again, it is the argon ion laser. But as it turned out, this new laser had a lot of disadvantages or imperfections.

Power and shapes of the beam

One really big disadvantage of this new laser is its power. After our best has been done (including cleaning of the cavity mirrors), we were still not able to get higher than to 6.8 W in multi-line mode (see [22]). But according to the basic characteristics, we should have been able to get up to 15 W. There is then the question, whether the laser was really running in the multi-line visible mode, or if it was set mechanically to the single-line mode at 514.5 nm (argon main wavelength). Then the maximum power would be only 7 W. Otherwise also an insufficient cooling should be taken into account.

As you can see from (3.2), the power of the laser is one of the leading parameters which can be improved to get the best result in the end. But the profile of the beam is maybe even more important. Ideally we expect Gaussian type shape, high and thin to affect only a few pixels. Then we would easily and more probably find in the final noise a prime beam profile, which we look for. That is why it was very surprising, when the measurements of the beam shapes at various powers were done (Fig. A.7). On the plot you can see average profiles of 10 min exposure time measurements (except for 5 W - 15 s and 6 W - 1 min) recounted to 1 s accu-

mulation through filters of optical density of 10. Up to 0.5 W the beam behaves as supposed. The height of the peak (or we can call it as a photon density) is proportional to the power of the laser. But as the power rises further, the shape is getting rather wider than higher (due to the thermal lensing effect). And also the center of the peak moves to the right. Thus much more pixels are affected and the density of photons is not rising any more. We loose in this unexpected way the contrast between the noise and the hypothetical axion signal.

A proposal for an amendment

Due to the previous description it is strongly recommended to start to look for a new laser. What characteristics should the new laser have? For the axion search we need at the first place a very high power (as many photons produced in a second as possible). But simultaneously it is still very important to have this power on the smallest possible area. Ideally the shape of the beam should look like the 0.5 W profile in Fig. A.7 or better.

For a practical purpose the wavelength belonging to the visible light is still a good solution. This is convenient for safety and alignment issues and also the CCD detector is sensitive to similar frequencies. Because of other elements involved, which are in some cases calibrated to 514.5 nm, the easiest way is to get an argon laser again. The higher percentage of the power is transfered into a single wavelength, the better.

For "laser beam bending" experiments, the geometrical stability is more important than the power. Therefore we have two possibilities. Either the new laser should also fulfill this condition, or we would get another, less powerful but very precise. In the first case, one could suggest to get the laser without any mechanically active optical element (e.g. PowerTracker).

The last thing is to decide, whether we are able to or want to buy a laser, or if it should be just borrowed from another institution or manufacturer itself as an advertising step. When we happen to find one, which could satisfy our requirements, the very next thing should be to run appropriate tests to be sure about its functionality before bringing it to SM18. It could be also interesting to share our problems and requirements with some producers, if they would not be able to develop a lasing device for us as a challenge.

The use of an amplifying or resonant cavity should be also discussed [18]. This cavity has to fulfill some basic, but very important parameters. It is very probable, that the diameter of the amplified beam will grow up and that the directions of the constituent rays will not be strictly parallel. Then this divergence should be small enough that the axions, which can arise from the conversion of the photons of this beam, would still go right in the pipe of the second magnet and to the detector. To increase the resolution, the appropriate focusing lens should be added before the CCD detector.

4.2 CCD detector

In our experiments we use the following CCD camera:

Manufacturer: Princeton Instruments
Type: VISAR
MODEL: LN/CCD-1100PB UV
SERIAL NO.: 3019409

It is liquid nitrogen cooled detector based on 2-dimensional CCD chip of resolution 330×1100 pixels from Princeton Instruments. The complete documentation can be found in manuals [23].

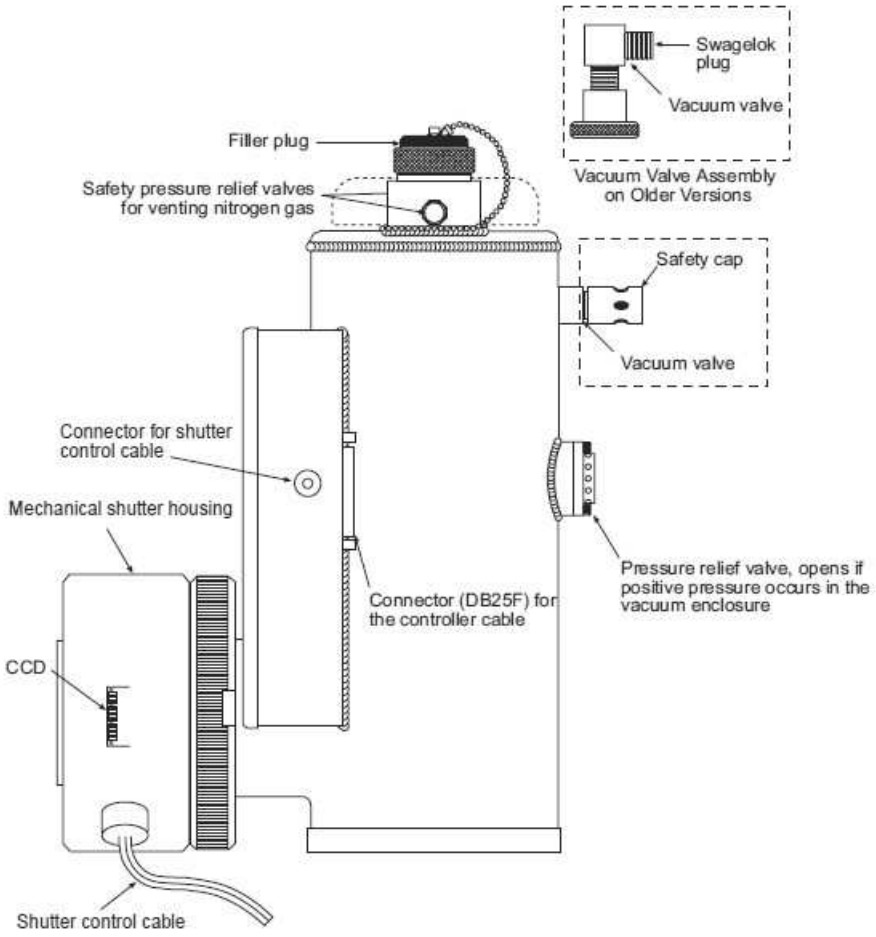

Figure 4.1: Liquid nitrogen cooled CCD, side view [23].

Calibration results

After all measurements had been completed, calibration tests were done. It was always necessary to know, how sensitive we were in the measurement. Besides the noise issues, the overall efficiency of the CCD should be checked. Ideally, one photon detected (i.e. one electron knocked free in the pixel) should mean one count in the spectrum. Let this ratio (detected to counted) call β, which in this simple case equals to 1. We must also consider the quantum efficiency η_q. For example, when (typically) η_q=50%, two photons coming to the detector would mean in average one photon detected and thus one count in the spectrum (consider that β still remains equal to 1).

The overall efficiency η of the experiment can be easily and approximately established. We let the laser beam of predetermined power P go through neutral density filters of known optical density Ω into the detector. By counting the area under the measured spectrum we get the number of photons detected (we expect β=1) $d \times \tau$ (where d stands obviously for the detection rate) during a known time interval τ (which is chosen long enough to suppress the background noise etc., but in the same time the CCD should not be oversaturated). And because from the power of the laser P we can simply calculate the presumed number of photons emitting to the camera direction within one second m (the first fraction in (3.2), in our case λ=514.5 nm, hence m=2.59x$10^{18-\Omega}P$), the overall efficiency η is then the ratio between detected d and emitted m photon rates:

$$\eta = \frac{d}{m} = \frac{hc}{P\lambda}d. \tag{4.1}$$

We expected that minimally the overall efficiency η is about 25% (including quantum efficiency of the camera η_q, reflection losses counted in transfer factor ρ etc.) considering that the detector service software displays rationally with β=1. But the results were quite surprising. From Tab. 4.1, one can easily calculate (errors included), that in average

$$\eta^{-1} = (185 \pm 25) \Longrightarrow \eta = (0.54 \pm 0.04)\%.$$

And that is alarming. Supposing that the η_q and ρ parameters are chosen rightly (we can set the lower bound as ρ=50%, that would mean we loose up to one half of the prime beam due to reflections etc.), we can take into account following formula:

$$\beta = \frac{\eta_q \rho}{\eta}. \tag{4.2}$$

This way we get to the result

$$\beta = (46 \pm 6), \tag{4.3}$$

which can be interpreted as follows: 1 count in the spectrum means in average 40-50 photons detected by the CCD. The question is why.

In general, that should mean our assumptions were wrong in some way. It is difficult to specify more precisely the ρ factor without a power-meter, but from a direct observation it is obvious, that we can't loose more than we expected. The overall efficiency about 1% of the camera would be very bad and really improbable. We would be rather blind than sensitive. On the top of it, η_q is one of the basic parameters of the CCD and if it was not consistent with the specified value, it would be a sign of a damage.

P[W]	τ[s]	Ω	$1/\eta$
0.01	5*30	10	244
0.02	20*30	10	265
0.05	30*20	10	166
0.10	120*5	10	143
0.20	10*60	12	200
0.50	10*60	12	161
0.50	20*30	12	150
0.50	40*15	12	142
1.00	40*15	12	193
2.00	40*15	12	150
5.00	1*15	12	220

Table 4.1: Overall efficiency of the current experimental setup

But another hidden matter of fact was pointed out by Dr. Pierre Pugnat, the member of OSQAR experiment, and the mystery or any other doubts were solved. The optical density Ω is much more wavelength dependent than was at first expected (due to an inattention) [24]. In fact, filters of nominal optical density Ω_n=5@633 nm behave like $\Omega\simeq$5.4@514 nm. Using two filters we get in total not Ω_n=10, but $\Omega\simeq$10.8, hence the final value of β in (4.3) should be multiplied additionally with the factor of 0.16 ($\simeq 10^{-0.8}$), thus we get to

$$\beta = (7 \pm 1)$$

and assuming also the high diffusivity of the absorbers and their distance from the detector (slightly more than L), we could get finally somewhere around $\beta\simeq$5.

This is much more realistic situation and an experimental verification of the parameter of the CCD called gain [23]. In fact, it is quite difficult to get one visible count in the final spectrum. Imagine photons falling on the CCD. Due to the quantum efficiency η_q, not all of them are registered, i.e. free electrons are not created. But now gain parameter becomes important, because it determines how many electrons are needed to produce one count. Typically, gain can be thought to be 5 electrons/count. And from the definition, it can be identified with our β parameter introduced at the beginning.

Other suggestions

Even though the camera would be fully functional and all our problems would be caused only by a human factor (e.g. improper handling, unknown parameters), it seems good to think about a possibility to get a more modern detector. It is true, that we got to know our device very well, still it has many disadvantages. The controller

> Manufacturer: Princeton Instruments
> MODEL NO.: ST-130
> SERIAL NO.: A0891256

is connected through a couple of cables to the computer, which has to be running in DOS mode because of the used ISA card and software:

> Princeton Instruments
> CSMA - CCD Spectrometric Multichannel
> Analysis Software
> (c) copyright 1989, 90, 91, 92, 93
> VERSION: 2.3c, October 7 1993.

During last measurements, many problems with the detector occurred. It was the end of the run and the measurements with another polarization of the beam should have been done. But it was not possible at all. For some reason the camera started to behave in unusual way. Either there was a terrible noise in the spectra, or no cosmics appeared. Though everything conceivable had been done, it was not possible to talk the camera over to work again in a short time. In my opinion there was at least a problem with the cable connection between the detector and its controller. The connectors require to be put into specific position where all the pins are joined properly.

There can be also other problems which are not uncovered yet. But all that can be said is that the detector is not fully reliable and not at all when measurements in limited time need to be done.

In the end it is important to say, that there are also other types of detectors (for example photomultiplier) upon which the discussion can be led about. There are always some pros and cons concerning photon and cosmic ray sensitivity, resolution etc. But the CCD (or maybe ICCD, which states for Intensified CCD) detector is still found as a good solution.

Cosmic rays

Another thing concerning the CCD is to be able to treat with the cosmic rays (or shorter term cosmics is often used). Cosmic rays are energetic particles having their origin in the universe. They are everywhere, coming from different directions. In the case they go through our CCD chip, they make these unavoidable marks in the final spectrum, which can be easily recognized.

At the moment we use, one could say, post-measurement filtering. There are two possibilities of how to get rid of those high and thin peak in the spectrum. The first one is to use the procedure implemented directly in the CSMA software. The second one, which was used in this case, is to make one's own script. There is a substantial advantage, that it is known exactly what the procedure is. There are simply no hidden properties and also some additional treatment can be done (e.g. statistical evaluation). The method and the level can be set, which of the peaks are cut and replaced with the average value of the background. The most simple and effective ways are cutting the peaks which exceed over some specified level (for flat spectra) or a derivative-based method. An example of the filtered spectrum is shown in Fig. A.1.

But we can also avoid the cosmic rays to influence the measurement with the help of some external shielding. It is the question, if it is possible to make some simple and effective steps to make the spectra look less like a forest. This filtration would allow us to extend the exposure time which would increase the sensitivity (or signal to noise ratio) of the measurement. But from another point of view, we are now able to run at 5 min expositions (what is quite enough) with acceptable level of cosmics.

After analyzing nearly 56 hours of measurements, quite a good statistics has been reached. In average, (10.5 ± 0.6) pixels are every minute affected by cosmic rays and need to be filtered (useful informations contained in this pixels have to be thrown away too). But that could be every of all 1100 pixels. We are in fact interested in a very small area of the whole chip, about 50-100 pixels in horizontal direction (depending on the beam width, see Fig. A.7), where the prime beam strikes on. To simplify all that thing and since the cosmics are distributed uniformly, if we consider, that we are concerned say in the eleventh of the whole chip (100 pixels), then, in average, only about 1 pixel important for us per minute is altered. Actually, the number is a little bit higher, because the cosmic ray affects also pixels nearby, but not so strongly to produce a removable peak.

4.3 Magnets

Blue LHC dipole magnets (standard cross-section in Fig. 4.2), which are available for us in SM18, are two of a small amount of devices we can be really proud of. The official names of the magnets we use are:

First magnet: HCLBB_001-IN002431
Second magnet: HCLBA_001-CR002868

Here are some basic parameters [25]. Cooled down to 1.9 K the magnetic field of 8.3274 T is due to the current of 11.85 kA circulating in superconducting wires induced (Fig. 4.3). The ultimate current should be 12.84 kA. During OSQAR experiments we pumped 12.85 kA into the dipoles, which means (supposing linear relationship) B_0=9.03 T. This strong and very homogeneous magnetic field should act at L=14.3 m.

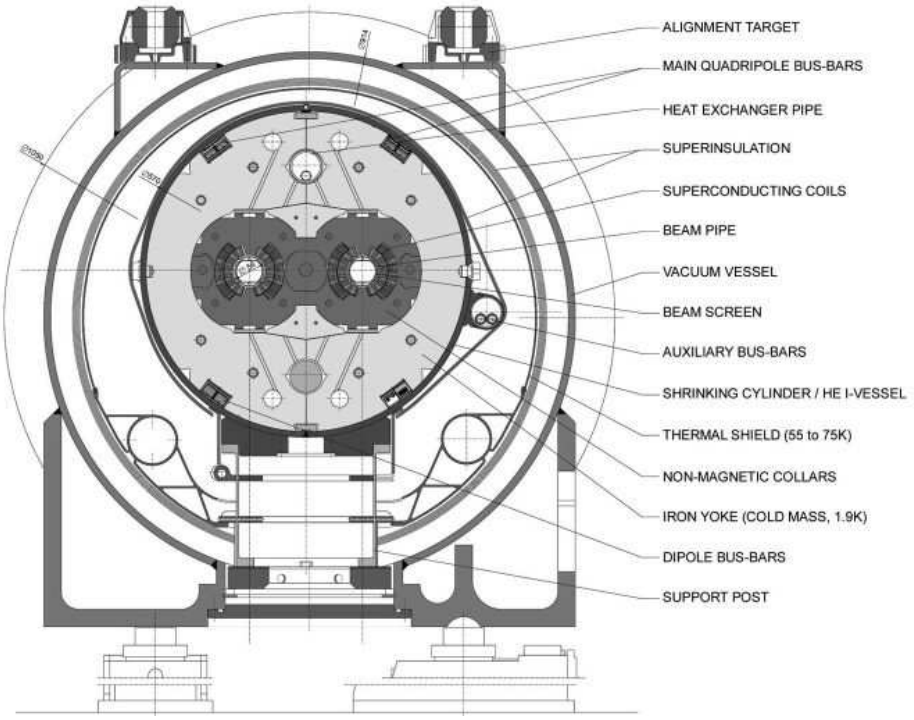

Figure 4.2: Standard cross-section of LHC dipole magnet.
source: <http://atlas.ch/atlas_photos/selected-photos/lhc/9906025_01_dipmag_diagram.jpg>

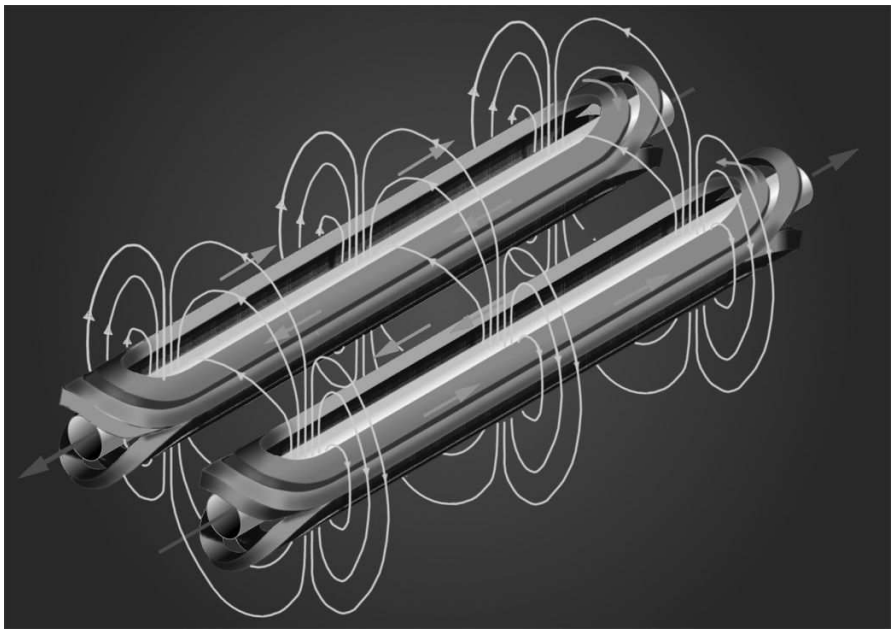

Figure 4.3: Magnetic field of LHC dipole. Configuration of superconducting cables around the pipes generating homogenous magnetic field is visible.
source: <https://lhc2008.web.cern.ch/lhc2008/inauguration/images/expo/lhc-pho-1998-325.jpg>

Chapter 5

Simulation

To have a more precise idea of how sensitive we are in our experiment, the simulation is a suitable way to resolve the problem. Especially, how many axions in average are needed to be detected in a minute to be sure, that something recognizable would be seen growing up from the noise.

Some background measurements (i.e. those, which were acquired when laser and magnetic field were turned off) were taken and divided into two equivalent parts. We got then two files containing measurements of the same total integration time (4hours) for every exposure time (30, 120 and 300 s). Then always one of this pair went through the simulation process. The beam width (ΔX=X2-X1=600-500=100) as well as the rate of how many photons (converted from axions and detected) arrive in a minute to the camera were chosen. For every count, this formula in C++ was used to find the pixel number where this one count will be added (since the line is short, the code was divided into more lines):

```
int R1=rand()%(X2-X1);
int R2=rand()%(X2-X1);
int randpix=X1+(R1+R2)/2+0.5;
```

It is in fact the sum of two equaly distributed random variables in the predetermined interval, which is a good approximation of the laser beam shape.

The final spectra were filtered from the cosmics (thus the real situation was considered) and summed together. You can see the result in Fig. A.8, A.10, A.12 and A.14. With the rate of generated axions (converted to photons and detected) rises also the beam shape from the noise. The subtraction of the other measurements (the second of each pair) from these altered with randomly added counts (signal minus background simulation) was also made. The results are in Fig. A.9, A.11, A.13 and A.15.

An approximate formula can be derived for the rate of counts needed for us to be able to see them in the spectrum (recognizable rate):

$$\nu = \frac{\sigma(\epsilon)}{\epsilon\sqrt{2\phi}}\Delta X, \tag{5.1}$$

where σ is a standard deviation of the noise in a single frame of exposure time ϵ, ϕ is the number of the frames used in the accumulation and ΔX is the length of the simulation interval.

To derive formula (5.1), consider following idea. In this simulation, the total number of photons detected by the camera is $\nu\phi\epsilon$. These counts are distributed

in the interval ΔX. The final shape is more or less a triangle. From that we know the height of the beam shape above the mean value of the noise. We need the top of this peak to be higher than the amplitude of the final noise A_n, thus

$$2\frac{\nu\phi\epsilon}{\Delta X} > A_n\sqrt{\phi} = \sigma\sqrt{2\phi},$$

where the square root of ϕ on the right side of the condition has the origin in the fit of Tab. 5.1 (a sample of calculated values, it is the typical noise cumulation property). The value (introduced in the table) x=0.5 fits best the small values of ϕ. For a high number of frames accumulated the values in Tab. 5.1 differ from the fit a little (maybe some filtering issues). The behaviour of the noise in frames of exposure time 30 s seems to fit best the curve of presumed exponent 0.5 (i.e. $\sqrt{\phi}$) on the nearly whole interval (see Fig. A.16). The noise is in this case very high (σ=14.74), but the rate of cosmics is low.

ϵ=300 s		ϵ=120 s		ϵ=30 s	
ϕ	$\sigma\phi^x$	ϕ	$\sigma\phi^x$	ϕ	$\sigma\phi^x$
1	7.618	1	5.012	1	14.74
2	10.94	2	7.216	2	20.90
3	13.52	3	8.894	3	25.38
4	15.75	4	10.32	4	29.42
5	17.72	5	11.58	5	32.70
6	19.53	6	12.74	6	36.08
7	21.20	7	13.79	7	38.82
8	22.79	8	14.78	8	41.39
9	24.30	9	15.72	9	44.00
10	25.75	10	16.61	10	46.24
20	37.61	20	24.06	100	146.1
30	47.24	30	30.15	200	204.2
40	56.08	50	40.65	300	248.7
50	64.92	100	64.17	400	287.9
60	73.28	150	84.70	500	320.9
70	81.22	200	103.6	600	351.8
80	88.31	250	121.0	700	376.8
90	93.89	300	137.0	800	404.5
100	98.08	360	157.6	900	441.6

Table 5.1: Summation of the noise: ϕ exponent fit

Now we can go back and compare these results with the simulation plots (Fig. A.8-A.15). As it is written in the keys of the plots, two examples were introduced, both of the same total exposure time 4 hours. In the first one we have 48 frames per 300 s of exposure time, in the second then 120 frames per 120 s. According to the equation (5.1), we can calculate

$$\nu_1 = 15.6\,\mathrm{min}^{-1} \qquad\qquad \nu_2 = 16.2\,\mathrm{min}^{-1}\,.$$

From the plots it is obvious, that it means the lower bound for the recognition of the signals generated by these rates. To be sure enough, double rates should be used.

Chapter 6

Estimation of the experiment sensitivity

Typical ranges of values of coupling constant g and mass m_p are shown in Fig. 6.1. To find the limits of our experiment, we start with the coupling constant.

When we look back to (3.1) and (3.2), we can evaluate these terms (in SI units after the dimension analysis is made) substituting the fixed parameters introduced in the previous section.

$$\Pi \simeq \left(\frac{B_0 L}{2}\right)^2 \frac{\hbar c}{\mu_0} g^2 \simeq 4169\, g^2 \frac{\hbar c}{\mu_0}\,\mathrm{T}^2\cdot\mathrm{m}^2 \simeq 1.05\times 10^{-16} g^2\,\mathrm{J}^2$$

$$n \simeq \left(\frac{B_0 L}{2}\right)^4 \frac{\hbar c}{2\pi {\mu_0}^2}\eta\lambda P g^4 \simeq 5.54\times 10^{-8}\eta\lambda P g^4\,\mathrm{J}^3\cdot\mathrm{m}^{-1} \tag{6.1}$$

Note that using Lorentz-Heaviside units, we would have

$$\text{Tesla} \sim \frac{\text{Mass}}{\text{Charge}\cdot\text{Time}} \Longrightarrow 1\,\mathrm{T} = 1\,\mathrm{T}\times\hbar c^2\sqrt{\hbar c\epsilon_0} \approx 195.35\,\mathrm{eV}^2$$

$$1\,\mathrm{m} = \frac{1\,\mathrm{m}}{\hbar c} \approx 5.0677\times 10^6\,\mathrm{eV}^{-1}$$

$$1\,\mathrm{T}\cdot\mathrm{m} = 1\,\mathrm{T}\cdot\mathrm{m}\times c\sqrt{\hbar c\epsilon_0} \Longrightarrow 1\,\mathrm{T}^2\cdot\mathrm{m}^2 = 1\,\mathrm{T}^2\cdot\mathrm{m}^2\times\frac{\hbar c}{\mu_0} \approx 9.8009\times 10^{17}\,\mathrm{eV}^2 \tag{6.2}$$

what is in perfect consistence with calculations (6.1) above. It is necessary to say, that to get the numerical values, fundamental constants used in the way of terms (6.2) have to be substituted in SI units and then converted to eVs.

If we put η=25% and λ=514.5 nm into (6.1), we get simply

$$n \simeq 7.12\times 10^{-15} P g^4\,\mathrm{J}^3 \tag{6.3}$$

Therefore, when we consider the limits rising from the equation (5.1), we should be able to detect axions with $g{>}2{\times}10^{-7}\,\mathrm{GeV}^{-1}{\simeq}1248\,\mathrm{J}^{-1}$ quite easily (for P=20 W, we have $n{\simeq}40\,\mathrm{min}^{-1}$ using (6.3)). But already for $g{\simeq}1{\times}10^{-7}\,\mathrm{GeV}^{-1}$, we would get $n{\simeq}2.6\,\mathrm{min}^{-1}$. In this case, to reach the desired confidence level, the total exposure time of about 10 days would be needed.

It is then quite difficult to enlarge the region because of the forth power of the coupling constant in (6.1). To get one order further, we would have to increase the power of the laser unimaginably. But a little bit beyond could get us an effective extension of the length of the magnetic field with the use of a cavity.

What if we let the light go through the first magnet k times, then the number of expected photons per second detected by the camera n in (6.1) would be after all $\lfloor (k+1)/2 \rfloor^4$ times higher (only one direction is important). But in fact, the cavity would effectively increase only the power of the laser (in terms of (6.1)). If we consider the reflectivity of the cavity mirrors [18, 26] to be R=1-δ=0.99998, the increased power in one direction would be P=P_0/δ=$5\times10^4\,P_0$. This would imply the shift of the measurement limits to $g>1\times10^{-8}\,\mathrm{GeV}^{-1}$.

But in [18] it is claimed, that also installation of another appropriate cavity to the second magnet (regeneration side) could be useful and that the overall increase factor in the signal power using present technology could be as large as $2/\delta\delta'$=10^{12}. In case the mirrors would not burn and would stand this high power, the limits can be finally set to be $g>1\times10^{-10}\,\mathrm{GeV}^{-1}$ (using current detection method).

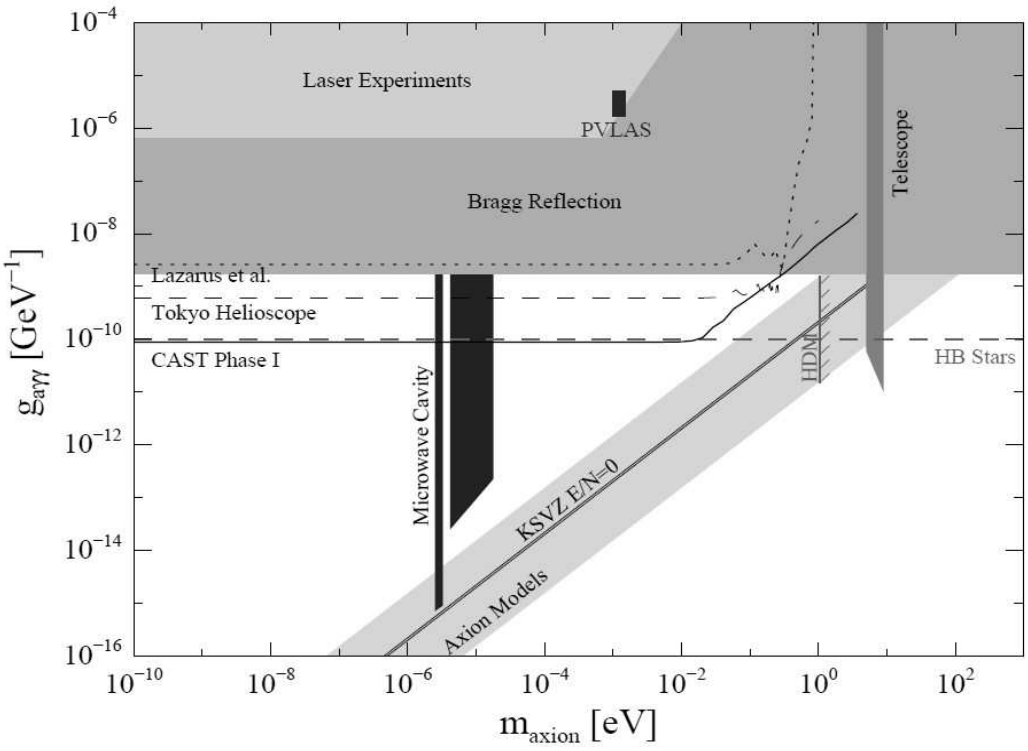

Figure 6.1: Exclusion plots [5]. Using our notation, coupling constant g in the parameter space versus pseudoscalar mass m_p (in the plot denoted as m_{axion}) is shown, where limits of different experimental techniques are denoted. The region predicted by theoretical models is marked as "Axion Models". The vertical line "HDM" indicates the hot dark matter limit for hadronic axions.

We can now estimate the limit of our experiment for a detection of pseudoscalars of a specific mass. The energy of a photon corresponding to the wavelength λ=514.5 nm is $\omega \simeq 2.4$ eV. To derive the simple formula (2.19), the condition that the term $m_p^2 L/4\omega$ is small (compared to unity) was assumed. Continuing in the previous calculation methods, we have $L=7.25\times10^7\,\mathrm{eV}^{-1}$, thus it is easy to obtain the limit $m_p \ll 2\times10^{-4}$ eV.

When the refractive index is taken into account, considering its reasonably achievable values by changing the pressure of the air (for normal conditions and Ar^+ laser main wavelength λ=514.5 nm we have $n_{r,N}^{(air)}$=1.00027024, [27, eq. (6a)]), the requirement $m_p \ll \omega$ has to be fulfilled (as was shown in the equation (2.22)). Hence, if we are able to set the refractive index precisely enough (in case of investigating pseudoscalars of the fixed specific mass m_p) to suppress the effects of the length L, i.e. $qL \simeq 0$ (see (2.20)), the limit previously established can be moved up to $m_p \ll 5\times10^{-2}$ eV.

To sum it up, when previously suggested improvements would be made, the limits could be moved according to Fig. 6.1 very close to the theoretically predicted axion region. In the end, in Fig. 6.2 there are preliminary results from the run in summer 2010 compared with the present limits of ALPS collaboration [13].

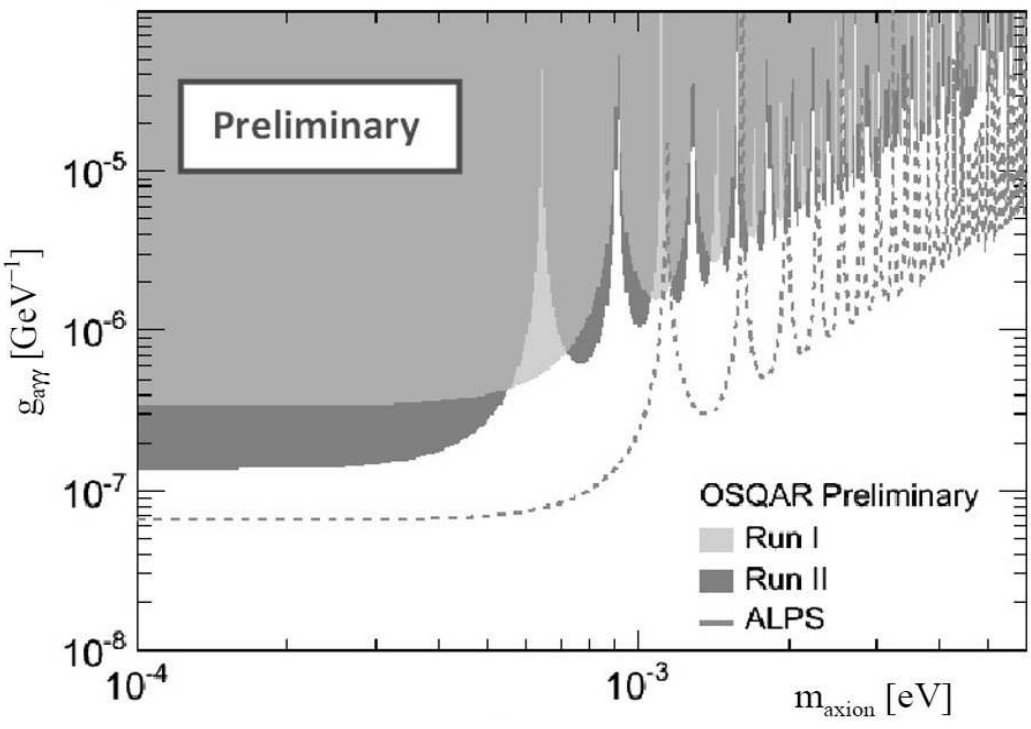

Figure 6.2: Preliminary results [2]. Exclusion limits of pseudoscalar and scalar particle search (which are very similar). Run I refers to the year 2007 [1], Run II states for the results from summer 2010.

Chapter 7

Calibration measurements

To find the optimal measuring modes related to the detection part of the setup, various tests including CCD detector were made. All in this chapter introduced results were obtained from measurements which took place in the low temperature laboratory at the Department of Low Temperature Physics at our faculty in Prague. The CCD detector has been borrowed from Division of Biomolecular Physics:

Manufacturer: Princeton Instruments
MODEL: LN/CCD-1024E/1
SERIAL NO.: J019321

with the controller

Manufacturer: Princeton Instruments
MODEL NO.: ST-130
SERIAL NO.: J0193512

It is again a liquid nitrogen cooled detector very similar to that one used at CERN, but in this case based on another two-dimensional CCD chip, EEV 256×1024. The documentation can be found in the same manuals [23].

The main tasks were aimed to find the appropriate exposure times and binning modes with respect to noise and cosmic rays level to gain as much signal as possible. It is also necessary to say, that in this chapter, all discussed spectra were primary acquired as the two-dimensional field, in contrast to all previous (in this work so called) frames, which originated from hardware binning, where all pixels in a one column (imagine the CCD chip as an array of X×Y pixels) were joined together to form one huge superpixel.

7.1 Cosmic rays

On the first place, the statistic in cosmic ray impact rate was made. The CCD chip side of the detector was tightly covered to prevent photons from the surroundings to involve in the measurement. Then the only signal detected were the cosmic rays and, in comparison to them insignificant, noise. The position spectra of various exposure times were acquired in sequence to see the evolution of the number of pixels affected by the cosmics to find the average impact rate. Full frame shots of exposure times 30, 120, 300, 600, 900 and 1800 s are shown in Fig. A.17. The

black points denote the accurate positions, where the cosmic rays went through the chip.

In this case, it is quite easy to find these positions. Because there is no background signal from other photons, the basic curve is a straight line a little disturbed mainly because of the readout noise. When the cosmic ray comes, the significantly high peak in the spectrum appears. It is then only necessary to find abnormally high values of counts (above the nearly flat field) and save the position. We can then calculate the total number of these black pixels N_{pix}. When more measurements are performed (in this case always more than 10 at all exposure times except for 900 and 1800 s), we can also evaluate the standard deviation $\sigma(N_{\mathrm{pix}})$. Particular values are shown in Tab. 7.1. With the use of linear fit of the general form y=kx (Fig. A.18), which is a good approximation when the chip is not already filled with cosmics, we get k=(0.34±0.02) s^{-1}. In this way we have found the average number of affected pixels rate to be

$$\overline{N_{\mathrm{pix}}} = (20 \pm 1)\,\mathrm{min}^{-1}.$$

It is necessary to say, that the result above is really important to understand in the meaning of something like the average expectation value.

$\epsilon[s]$	N_{pix}	$\sigma(N_{\mathrm{pix}})$
1	5	4
30	13	13
120	48	20
300	94	29
600	199	36
900	264	46
1800	680	75

Table 7.1: Number of affected pixels by the cosmic rays in average

The number of cosmic rays detected is a random variable with Poisson distribution. But the number of pixels affected by a single cosmic can change from case to case and is also random (typically 2-3). Analyzing the values in Tab. 7.1, we can find, that the standard deviation of the total number of pixels hit satisfies the relation

$$\sigma(N_{\mathrm{pix}}) \simeq 3\sqrt{N_{\mathrm{pix}}}\,.$$

Thus we can expect, that during a random measurement of an exposure time ϵ, the number of pixels on the whole area of the CCD chip, which will be affected by the cosmic rays, would be

$$N_{\mathrm{pix}} = k\epsilon \pm 3\sqrt{k\epsilon}\,.$$

It must be also said, that cosmic ray activity differs e.g. during the time or with the elevation above sea-level, but the previous results hold (at least approximately) true.

7.2 Noise

After we get rid of the cosmic rays, we are able to analyze the noise issues. It will be discussed, (i) which exposure times and binning modes to use, (ii) if it is better to sum together more spectra containing less signal, or to expose for a long time, (iii) if it is better to use a hardware binning and (iv) how many pixels should then form the superpixel.

At first we start with the readout noise. Suppose that the CCD chip side of the detector was properly covered again so no photons coming from outside can affect the measurement. If short exposure time is set, then a contribution from the potential thermal noise is reduced too, thus really only the readout noise can be recorded on the final spectrum. To estimate its value, one of the possible methods is to subtract these two different "bias" spectra and then to calculate the standard deviation of this difference [28]. Because two spectra were subtracted, the result should be finally divided by the square root of two. Ten full-frame shots of exposure time 1 s were taken and underwent this procedure. For the whole array, we get then the readout noise

$$\sigma_{RN} = (0.359 \pm 0.006)\,\text{count}\,.$$

An example of a single row and the sum of the rows of one zero-exposure-time (i.e. very short exposure time so the contributions from other noise sources are negligible) or so called bias measurement are shown in Fig. A.19 and Fig. A.20 respectively.

When we put together the readout noise with its dependence on the hardware binning and use the same procedure as before, we get values in Tab. 7.2. The numbers in the first column named as (C-R) mean, how many Columns and Rows were binned together or alternatively the dimensions of the superpixel formed from C*R pixels. To make this more certain, e.g. for 1-2 binning mode, every pair of neighbouring rows creates one wider row. The number in parentheses at the sigma symbols means the exposition time (1 or 10 s);

(C-R)	$\sigma_{RN}^{(1)}$[counts]	$\sigma_{RN}^{(10)}$[counts]
1-1	0.359 ± 0.006	0.38 ± 0.04
1-2	0.338 ± 0.003	0.33 ± 0.01
1-4	0.433 ± 0.009	0.486 ± 0.003
2-1	0.496 ± 0.009	0.46 ± 0.03
4-1	0.44 ± 0.02	0.42 ± 0.02
2-2	0.431 ± 0.006	0.373 ± 0.004
4-4	0.385 ± 0.003	0.360 ± 0.002

Table 7.2: Readout noise and its dependence on the used hardware binning mode.

Pixels can be compared with a deep well, where charges are cumulated and stored for the exposure time before they are read (not precisely but with an uncertainty which shows itself as the readout noise). When pixels are binned together to form the superpixel, one can imagine that just one greater well is

created. Advantage of this feature can be recognized, when small signals need to be detected.

To proceed further with the noise analysis, the covering of the CCD chip side of the detector was partly removed to modify the flat zero-exposure-time spectra with some signal. Whatever procedures are made with the spectra (summation etc.), it is always important to have the possibility to extract the noise from the final curve to calculate its standard deviation. Because the spectra differ from each other due to fluctuations of various type, it is convenient to use the properties of DFT (Discrete Fourier Transformation), defined as (forward and inverse transform respectively)

$$X_k = \sum_{n=0}^{N-1} x_n e^{-2\pi i \frac{kn}{N}} \qquad\qquad x_n = \frac{1}{N} \sum_{k=0}^{N-1} X_k e^{2\pi i \frac{kn}{N}}\,, \tag{7.1}$$

where N is the number of spectrum points of values x_i and X_i is then the transformed sequence. From (7.1) we obtain

$$x_n = \frac{1}{N} \sum_{k=0}^{N-1} \left(\sum_{l=0}^{N-1} x_l e^{-2\pi i \frac{kl}{N}} \right) e^{2\pi i \frac{kn}{N}} = \frac{1}{N} \sum_{k,l=0}^{N-1} x_l e^{\frac{2\pi k(l-n)}{iN}} =$$

$$= \frac{1}{N} \sum_{k,l=0}^{N-1} x_l \cos\left[\frac{2\pi k(n-l)}{N}\right] = \tag{7.2}$$

$$= \frac{1}{N} \sum_{k=0}^{N-1} \left[\cos\left(\frac{2\pi kn}{N}\right) \sum_{l=0}^{N-1} x_l \cos\left(\frac{2\pi kl}{N}\right) + \sin\left(\frac{2\pi kn}{N}\right) \sum_{l=0}^{N-1} x_l \sin\left(\frac{2\pi kl}{N}\right) \right]. \tag{7.3}$$

The formula (7.2) looks very simple, but actually it is quite time-consuming to evaluate it numerically as it stays. Thus (7.3) was used to analyze the spectra, because it is much faster (the trigonometric functions do depend only on two indices). Of course to get shorter evaluating times, FFT (Fast Fourier Transform) algorithms could be used (not essentially necessary here). And what is important, using DFT it is possible to extract arbitrary parts of the spectra depending on frequencies (while omitting the appropriate k values from the sum in (7.3)), e.g. low frequencies can be suppressed to retrieve only the noise. To conceal some unfavourable effects of the transformation occurring at the margins of the spectra, the DFT was performed on a greater interval than given by the width of the chip (in fact three time greater to cover both sides).

The results for various binning modes are shown in Tab. 7.3 and Tab 7.4. Values in the (C-R) column mean again the number of Columns and Rows of the CCD chip binned together by hardware. From every (super)pixel created in this way, 66.7 counts were subtracted. This value was estimated from analyzing the bias measurements (as can be seen in Fig. A.20). Every read pixel contains this number of counts as defaults. Then all rows from a single measurement were summed together to produce the final spectrum corresponding with the chosen binning mode. The total detected signal S is then the area under this spectrum and with the use of DFT we can extract the noise to calculate its standard deviation σ_N. As a criterion for the efficiency of the binning method concerning the signal gain, the overall signal to noise ratio (S/σ_N) was calculated. The subscripts H and L in the table headers are introduced to distinguish between

values, when High and Low levels of incoming light were used (particular numbers of photon rates are written in the table descriptions).

According to [23], the hardware binning is useful to improve the signal to noise ratio when low photon rates are expected and in contrary, it should be not very convenient for high signals detection. Examining Tab. 7.3 (high light level signals), we find out that there is no special reason to use any of the tested binning modes. On the other hand, for low signal (Tab. 7.4) there are some candidates, especially modes 1-2 and 1-4 and eventually also 1-8 look very promising. In case of 1-2 binning, the highest light level signal (1.35×10^6 counts) is detected. The lowest noise sigma (8.91 counts) was measured using 1-4 mode.

(C-R)	$S_H[10^6$ counts]	$\sigma_{N,H}$[counts]	$S_H/\sigma_{N,H}[10^3]$
1-1	188	237	791
1-2	165	213	772
1-4	117	162	722
2-1	151	255	593
2-2	103	189	545
4-1	126	287	438
4-4	95.2	241	395

Table 7.3: Signal to noise ratio ($S_H/\sigma_{N,H}$) and its dependence on the used hardware binning mode at high signal level (exposition time 60 s, total average signal rate ≈12 counts/pixel/second).

Besides the numbers in the tables, we can compare the binning modes using a plot. From Fig. A.21, it is obvious that using 1-2 mode the signal gain is significantly higher than with no binning used. It is also important to say that the last measurements dependent on the outside light (results in Tab. 7.3 and Tab 7.4) may include some uncertainties arising from possible daylight intensity scatter.

(C-R)	$S_L[10^6$ counts]	$\sigma_{N,L}$[counts]	$S_L/\sigma_{N,L}[10^3]$
1-1	1.26	10.9	116
1-2	1.35	9.59	141
1-4	1.27	8.91	143
1-8	1.19	8.99	132
2-2	1.28	12.3	104
2-4	1.26	14.3	88
2-8	1.23	11.4	108
4-4	1.21	17.3	70

Table 7.4: Signal to noise ratio ($S_L/\sigma_{N,L}$) and its dependence on the used hardware binning mode at low signal level (exposition time 300 s, total average signal rate ≈0.02 counts/pixel/second).

To complete this section, there are also other two important sources of the noise.

The thermal noise increases with time and depends on the temperature T of the CCD chip. According to the controller manual [23], at T=-50 °C the average dark charge value is approximately 0.5 counts/pixel/second (≈3-6 electrons) and it is reduced by a factor of ∼2 for every 7 °C. The spectra are measured at very low temperatures (typically -120 °C) thus the thermal noise is negligible even at 30 min expositions. The sigma of the thermal noise σ_{TN} is equal to the square root of the dark charge.

The photon shot noise depends on the amount of the light hitting the chip [28]. Standard deviation σ_{PN} is then the square root of the total number of photo-electrons knocked free in each pixel. In our case this can be significant, dependent on the exposure time and photon regeneration rate and is of course the main source of the noise in the preceding measurements.

7.3 Recommendation

Taking the previous results into the consideration, the optimal measuring procedure can be established.

In our case, if we were not very lucky, we would need to detect very low light level signals. It is easy to consider, that it is convenient to make as long expositions as possible. If the gain of the controller was 5 electrons/count, exposing the CCD for a time too short to product sufficient amount of electrons in a single pixel would cause no desirable counts in the spectrum. But on the other side, we cannot let the cosmic rays to cover all the chip area with the sharp peaks so the upper limit for the exposure time is needed to be set. From Fig. A.17 we can see, that for ϵ=30 min the measurement is still possible, but the number of the black points is not exactly small. But we have to also assume, that from the whole chip only a square of size about 100×100 pixels is interesting (or maybe smaller), where the focused laser beam would strike on. And what is also important is then the binning mode, which we would like to use. The greater would be the superpixel, the shorter should be the exposure time because of the cosmic rays (the black points in Fig. A.17 would be greater).

To sum it up, it is recommended to set the hardware binning mode to 1-2, exposure time to 900 s (15 min) and make some acquisitions. After they are filtered from cosmics, to improve the S/σ ratio the spectra are summed together and the rows of the resulting spectrum are then summed too to produce the final position spectrum, which can be searched for containing some interesting signal.

Chapter 8

Epilogue

Although no axions were so far observed, OSQAR is a promising and viable experiment. It is very probable, that much work is needed to be done before some interesting results (positive or negative) will be obtained.

It is one of the experiments, where no one really knows what to expect. The first mystery is if axions (or eventually other hypothetical particles, which were mentioned) do really exist. In case they do, in which mass or coupling constant region they should be searched? Although there are some theoretical models, the whole available range shall be probed. Because what exist on the paper or in the minds of theoreticians, does not unfortunately need to exist in reality. It is not certain, if this experiment is allowed to make some important positive discovery, if it is able to get far enough. It will be a long journey, on which I hope much good work will be done and thus whatever results will be obtained, they would be valuable. This is the research, everything is so uncertain.

As other theories, which played some role in the past, the existence of axion like particles has certainly its sympathizers and doubters. The proof for this elegant solution of many present problems has not been found yet, though many experiments attempted to. But only well-prepared experiment can act as a reliable judge. OSQAR experiment is basically very simple (at least the idea of photon regeneration), what I like: laser light, magnet field and CCD detector. But it has showed up that it won't be actually so easy. Many improvements have to be done and over many difficulties it is needed to get.

Axions as a solution are so graceful, that I believe in their existence. But what is the truth? We cannot choose but continue in the experiment. Next run of OSQAR experiment is planned in summer 2011, when experiences obtained in previous runs will be used to get a little bit further again.

Conclusion

In the preceding chapters, experiment OSQAR was introduced, informations about its current status and latest results were presented and the feasible limits found.

In 2010, the discovery potential of the OSQAR photon regeneration experiment has been significantly improved by the simultaneous use of two LHC dipoles. The sensitivity obtained for light pseudoscalar and scalar particles search reached the foreseen target and is surpassed only by the new results recently published by the ALPS experiment at DESY [2, 13].

To improve the limits of the experiment, two main targets are considered to be aimed at. In the first place, it is the increase in the power of the laser, proper focusing lens installation and integration of the resonant cavity into the system. This is the main goal and great challenge for the future (during runs in 2011 and 2012). Secondly, it is the use of a new state-of-the-art CCD detector connected with an increase of the gain and quantum efficiency and suppression of the noise. To reduce the background signals, a proper shielding should be considered.

Concerning the detection modes, necessary experiences were obtained thanks to the measurements with the CCD detector in Prague within the frame of this work. The great advantage of the measurement in 2D mode was tested and proved, noise sources and cosmic rays detection analyzed and optimal exposure time and binning mode chosen. Some of these parameter are detector model and focusing possibility dependent, so the calibration measurements could be repeated and quickly processed while everything is already prepared and studied. The idea of using another type of the detector than the CCD was mentioned and should be discussed.

If there will be any possibility, more ample tests should be done regarding the bending of the laser beam in the presence of the strong magnetic field and eventual residual gases. This new investigation should bring some light into this hopefully temporary mystery and decide, if there is really some new discovery. It has been shown by the calculation, that the potential photon charge effect would be much weaker than the observed one considering present astrophysical boundaries. Thus other explanations should be proposed. For this measurement, the stability of the laser beam is the primary task.

Bibliography

[1] Pugnat, P., Duvillaret, L., Jost, R., Vitrant, G., Romanini, D., Siemko, A., Ballou, R., Barbara, B., Finger, M., Finger, M., Hošek, J., Král, M., Meissner, K. A., Šulc, M., and Zicha, J. Results from the OSQAR photon-regeneration experiment: No light shining through a wall. *Phys. Rev. D 78*, 9 (Nov. 2008).

[2] Pugnat, P., et al. OSQAR Status Report. *CERN-SPSC-SR-074* (Nov. 2010).
URL: <http://cdsweb.cern.ch/record/1308470/files/SPSC-SR-074.pdf>.

[3] Pugnat, P., et al. OSQAR Proposal. *CERN-SPSC-2006-035* (Nov. 2006).
URL: <http://cdsweb.cern.ch/record/997763/files/spsc-2006-035.pdf>.

[4] Pugnat, P., et al. Letter of Intent. *CERN-SPSC-2005-034* (Oct. 2005).
URL: <http://cdsweb.cern.ch/record/896649/files/spsc-2005-034.pdf>.

[5] Battesti, R., et al. Axion searches in the past, at present, and in the near future. In *Lect. Notes Phys.* [8], pp. 199–237.

[6] Van Bibber, K., Dagdeviren, N. R., Koonin, S. E., Kerman, A., and Nelson, H. N. Proposed experiment to produce and detect light pseudoscalars. *Phys. Rev. Lett. 59* (1987), 759–762.

[7] Weinberg, S. A New Light Boson? *Phys. Rev. Lett. 40*, 4 (Jan. 1978), 223–226.

[8] Kuster, M., Beltran, B., and Raffelt, G., Eds. *Axions: Theory, Cosmology, and Experimental Searches*, vol. 741 of *Lect. Notes Phys.* Springer, 2008.

[9] Peccei, R. D., and Quinn, H. R. CP Conservation in the Presence of Pseudoparticles. *Phys. Rev. Lett. 38*, 25 (June 1977), 1440–1443.

[10] Baker, C. A., Doyle, D. D., Geltenbort, P., Green, K., van der Grinten, M. G. D., Harris, P. G., Iaydjiev, P., Ivanov, S. N., May, D. J. R., Pendlebury, J. M., Richardson, J. D., Shiers, D., and Smith, K. F. Improved Experimental Limit on the Electric Dipole Moment of the Neutron. *Phys. Rev. Lett. 97*, 13 (Sept. 2006).

[11] Wilczek, F. Problem of Strong P and T Invariance in the Presence of Instantons. *Phys. Rev. Lett. 40*, 5 (Jan. 1978), 279–282.

[12] Zavattini, E., et al. Experimental Observation of Optical Rotation Generated in Vacuum by a Magnetic Field. *Phys. Rev. Lett. 96*, 11 (Mar. 2006).

[13] Ehret, K., et al. New ALPS results on hidden-sector lightweights. *Physics Letters B 689*, 4-5 (2010), 149–155.

[14] Battesti, R., et al. The BMV experiment: a novel apparatus to study the propagation of light in a transverse magnetic field. *The European Physical Journal D - Atomic, Molecular, Optical and Plasma Physics 46* (2008), 323–333.

[15] Zioutas, K., et al. First Results from the CERN Axion Solar Telescope. *Phys. Rev. Lett. 94*, 12 (Apr. 2005).

[16] Cameron, R., Cantatore, G., Melissinos, A. C., Ruoso, G., Semertzidis, Y., Halama, H. J., Lazarus, D. M., Prodell, A. G., Nezrick, F., Rizzo, C., and Zavattini, E. Search for nearly massless, weakly coupled particles by optical techniques. *Phys. Rev. D 47*, 9 (May 1993), 3707–3725.

[17] Adler, S. L., Gamboa, J., Mendez, F., and Lopez-Sarrion, J. Axions and 'Light Shining Through a Wall': A Detailed Theoretical Analysis. *Annals Phys. 323* (2008), 2851–2872.

[18] Sikivie, P., Tanner, D. B., and van Bibber, K. Resonantly Enhanced Axion-Photon Regeneration. *Physical Review Letters 98*, 17 (Apr. 2007).

[19] Barnett, S. M. Resolution of the Abraham-Minkowski Dilemma. *Phys. Rev. Lett. 104*, 7 (Feb. 2010).

[20] Jary, V. SPE-tools Project.
URL: <`http://kmlinux.fjfi.cvut.cz/~jaryvlad/spe-tools.html`>, 2010.

[21] Altschul, B. Bound on the Photon Charge from the Phase Coherence of Extragalactic Radiation. *Phys. Rev. Lett. 98*, 26 (June 2007).

[22] Coherent Lasers. Innova 400 Series Specifications.
URL: <`http://www.laserinnovations.com/innova400.htm`>.

[23] Princeton Instruments, Roper Industries. *LN/CCD Detector manual, ST-130 Controller Operation manual and CSMA User's manual.*
URL: <`ftp://ftp.princetoninstruments.com/public/Manuals/PrincetonInstruments/Archived/`>.

[24] Thorlabs. Absorptive Neutral Density Filters spec.
URL: <`http://www.thorlabs.de`>.

[25] CERN. LHC online Equipment Catalogue.
URL: <`https://edms.cern.ch/nav/`>.

[26] Kral, M. *Feasibility Study of an Experiment to Measure Vacuum Magnetic Birefringence.* PhD thesis, Czech Technical University in Prague, 2007.

[27] Bönsch, G., and Potulski, E. Measurement of the refractive index of air and comparison with modified Edlén's formulae. *Metrologia 35* (1998), 133–139.

[28] Michael Richmond. Readout Noise, and Total Noise.
URL: <`http://spiff.rit.edu/classes/phys445/lectures/readout/readout.html`>.

List of Tables

List of Figures

Attachments

A Plots

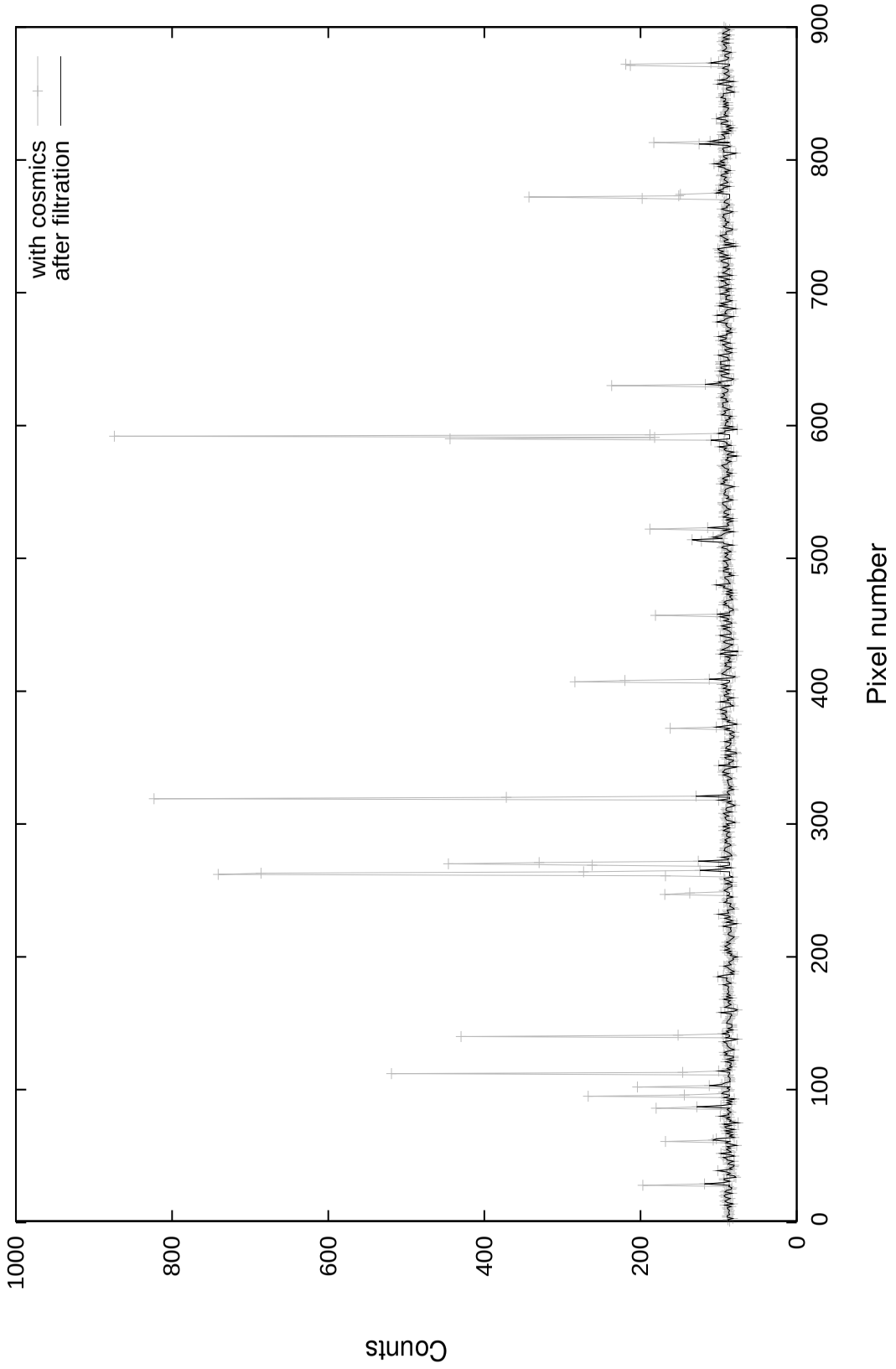

Figure A.1: Spectrum sample (1 frame with filtration of cosmics).

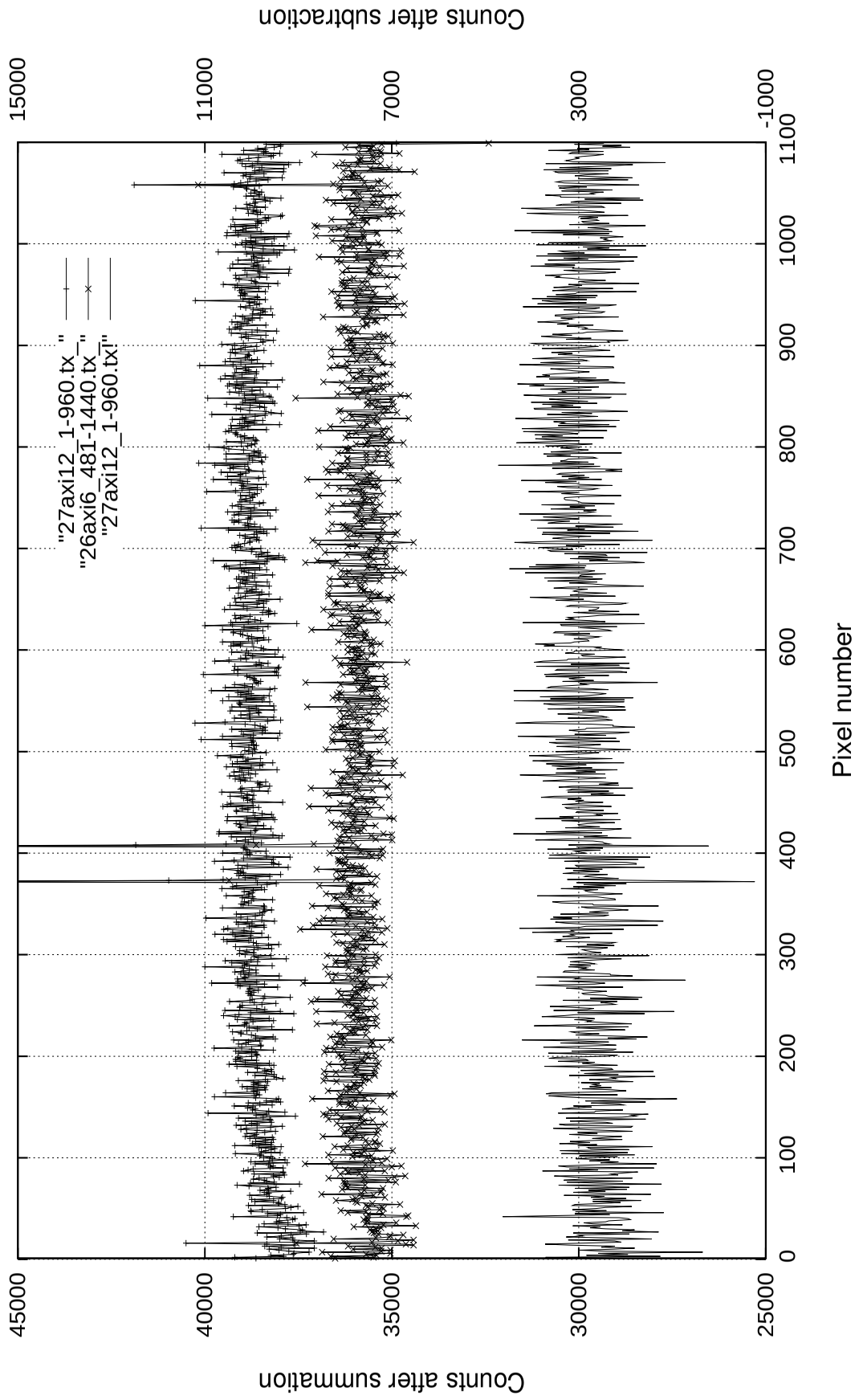

Figure A.2: Results - Total exposure time 8 hours (960 frames per 30 seconds).

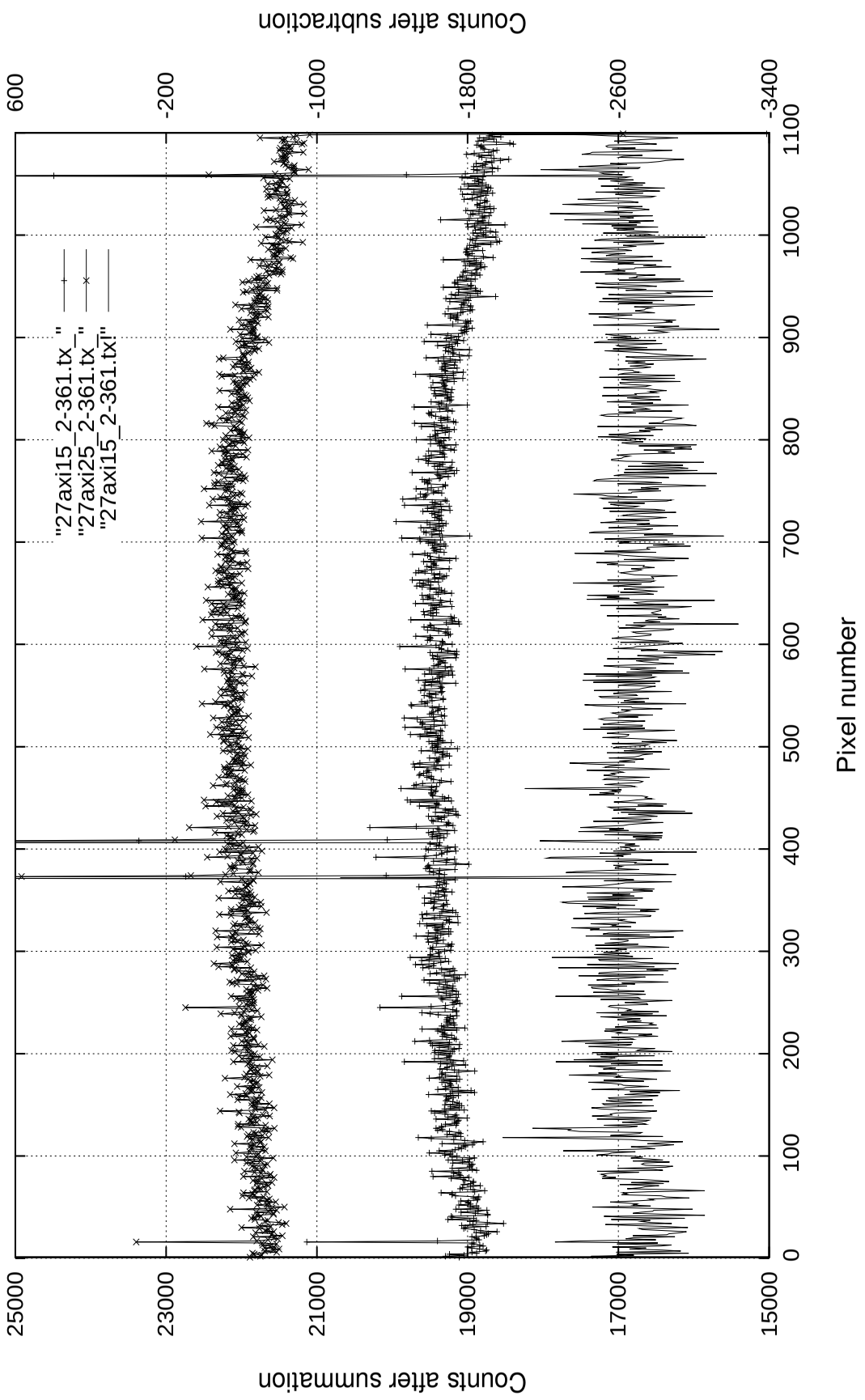

Figure A.3: Results - Total exposure time 12 hours (360 frames per 2 minutes).

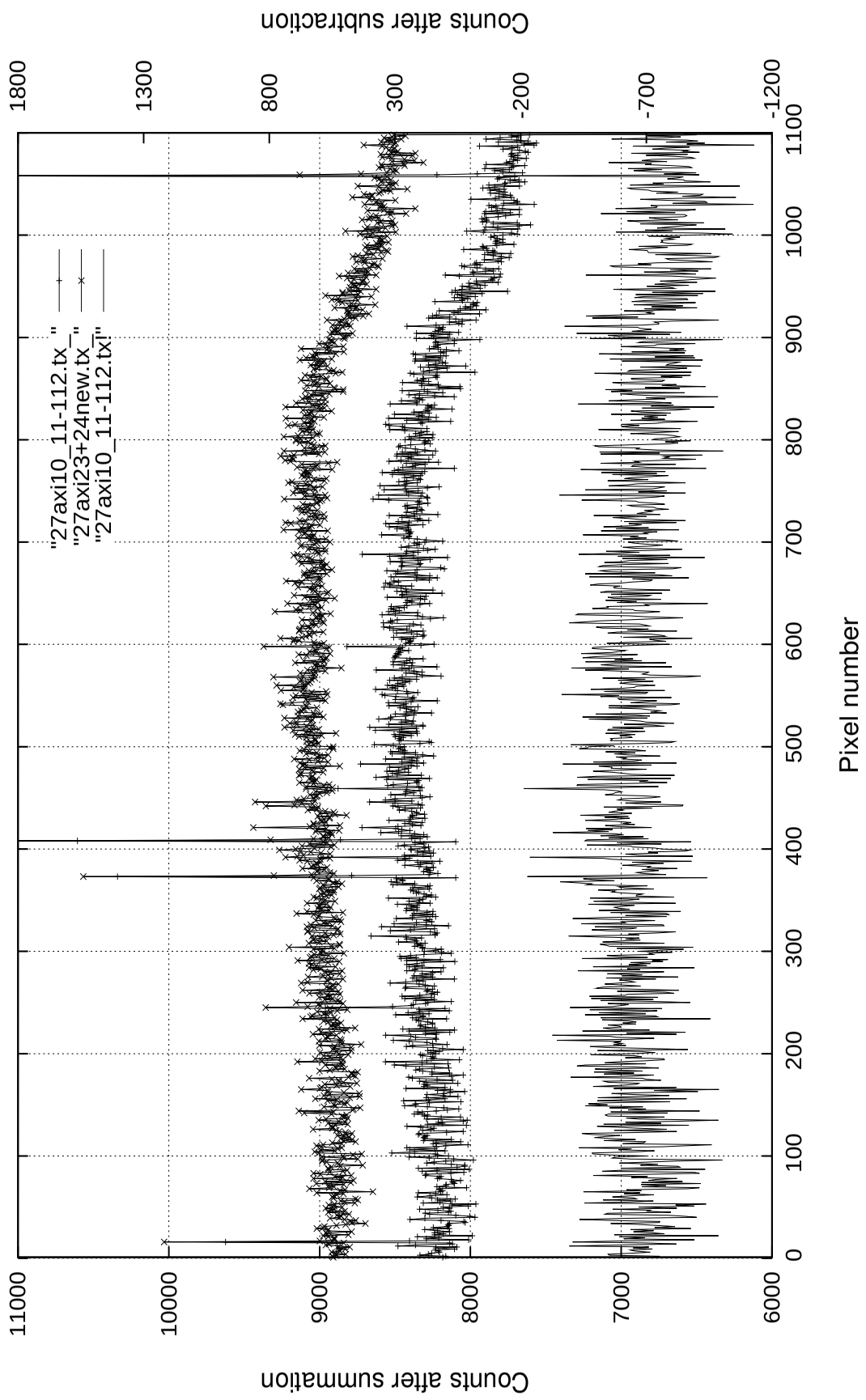

Figure A.4: Results - Total exposure time 8.5 hours (102 frames per 5 minutes).

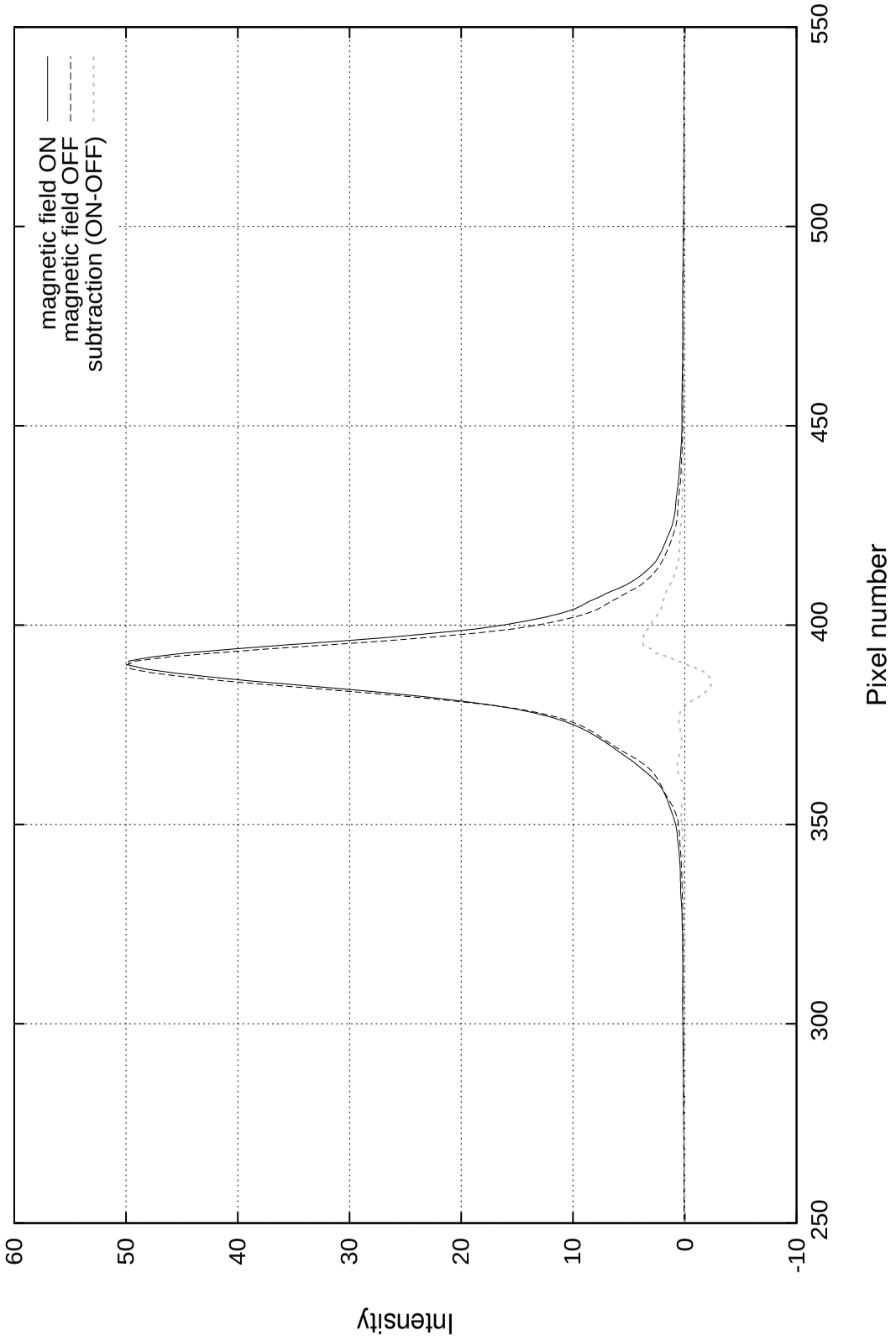

Figure A.5: Laser beam shift (50 frames accumulation).

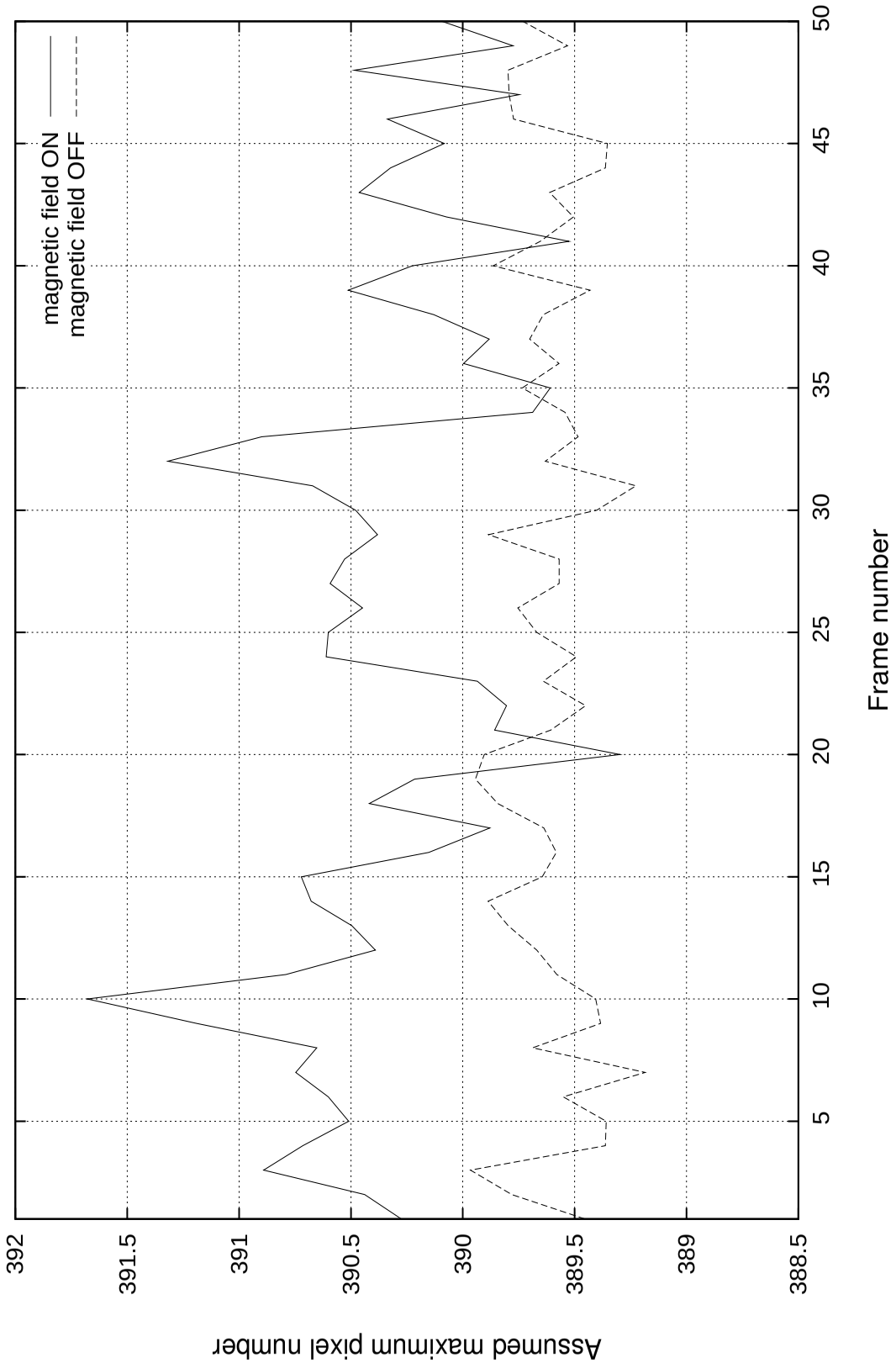

Figure A.6: Laser beam shift (50 frames separately).

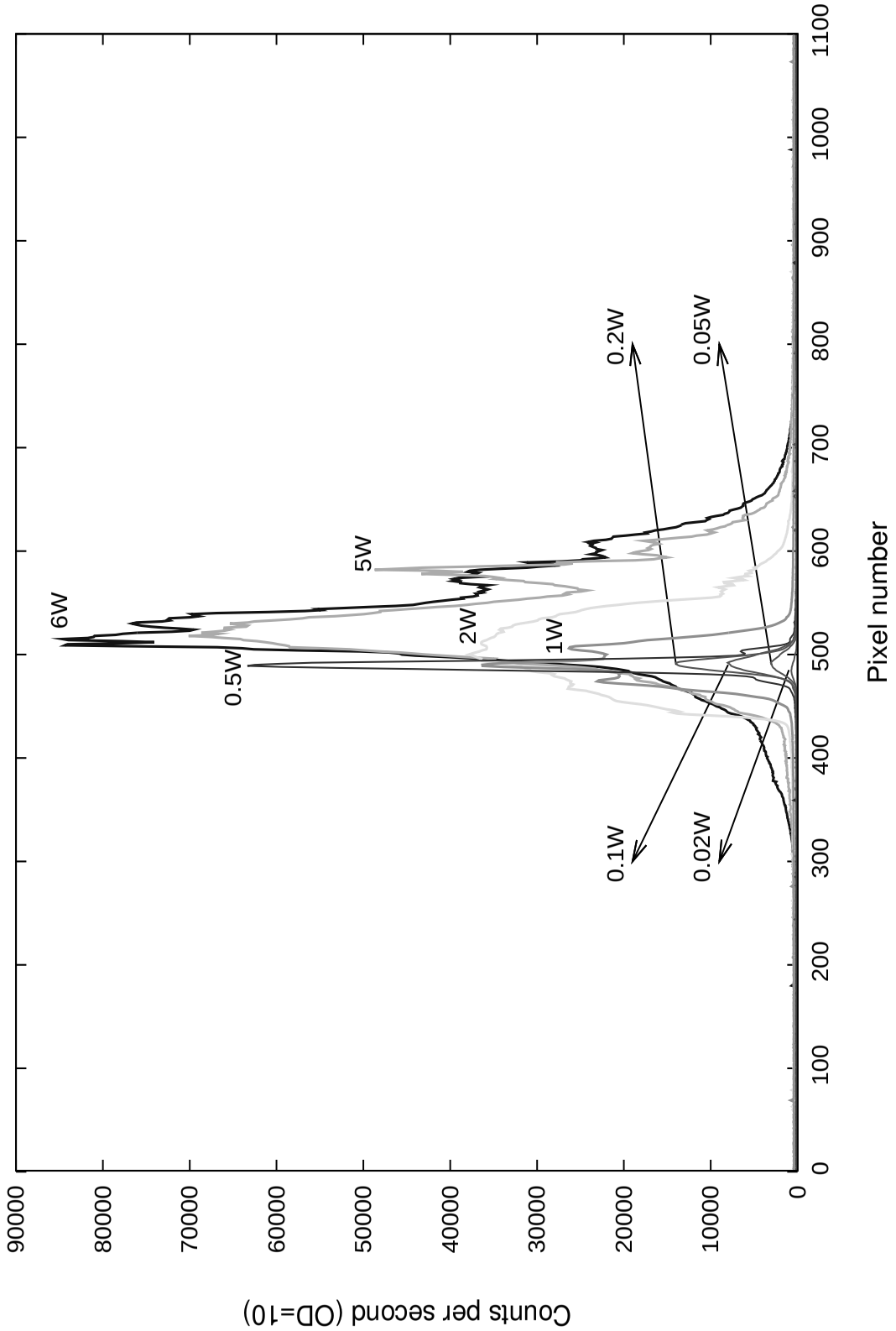

Figure A.7: Shapes of the laser beam.

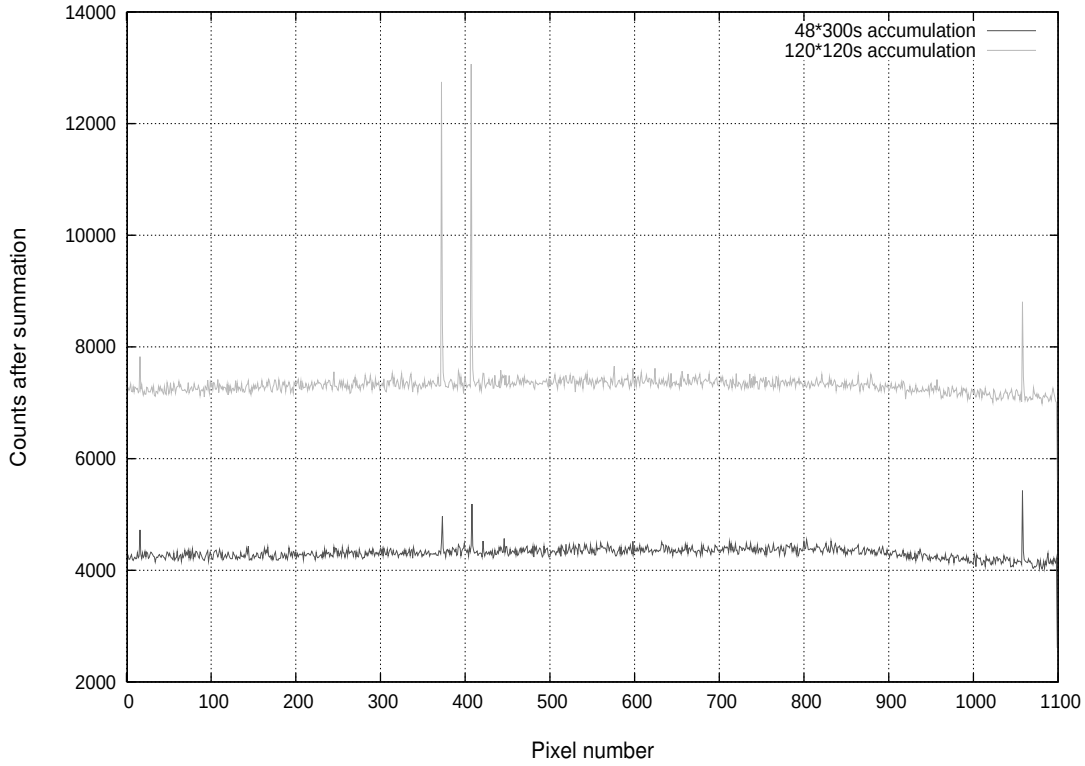

Figure A.8: Simulation - no axions.

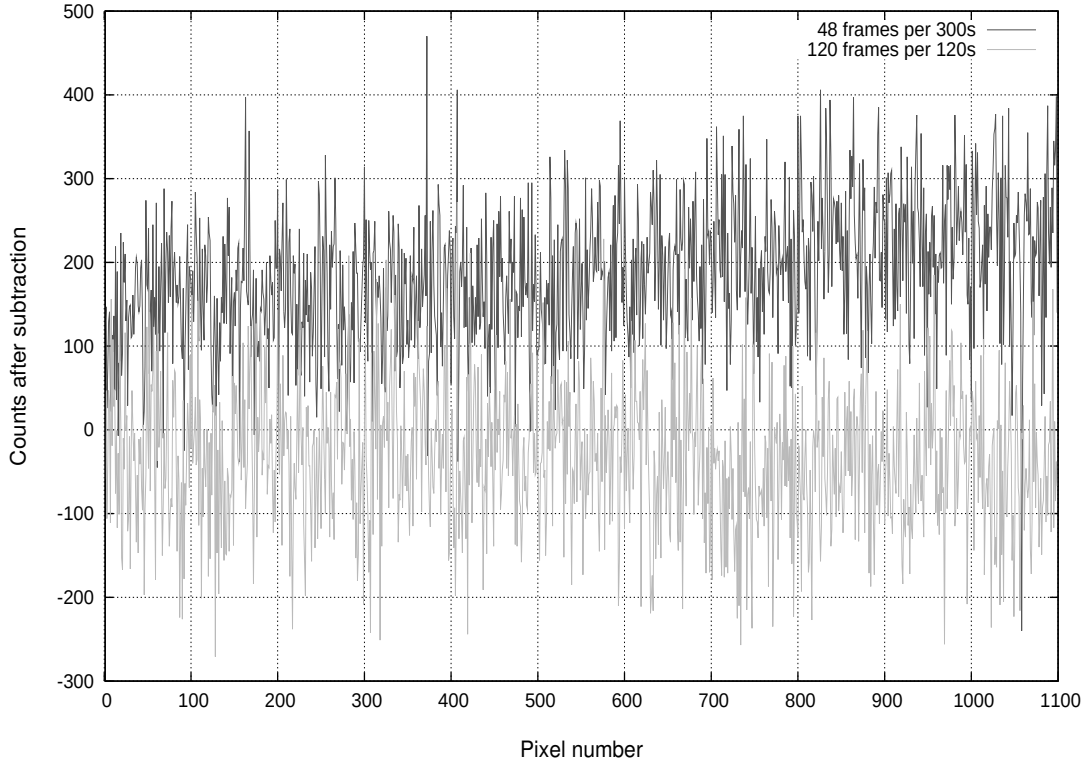

Figure A.9: Simulation - no axions (BG subtracted).

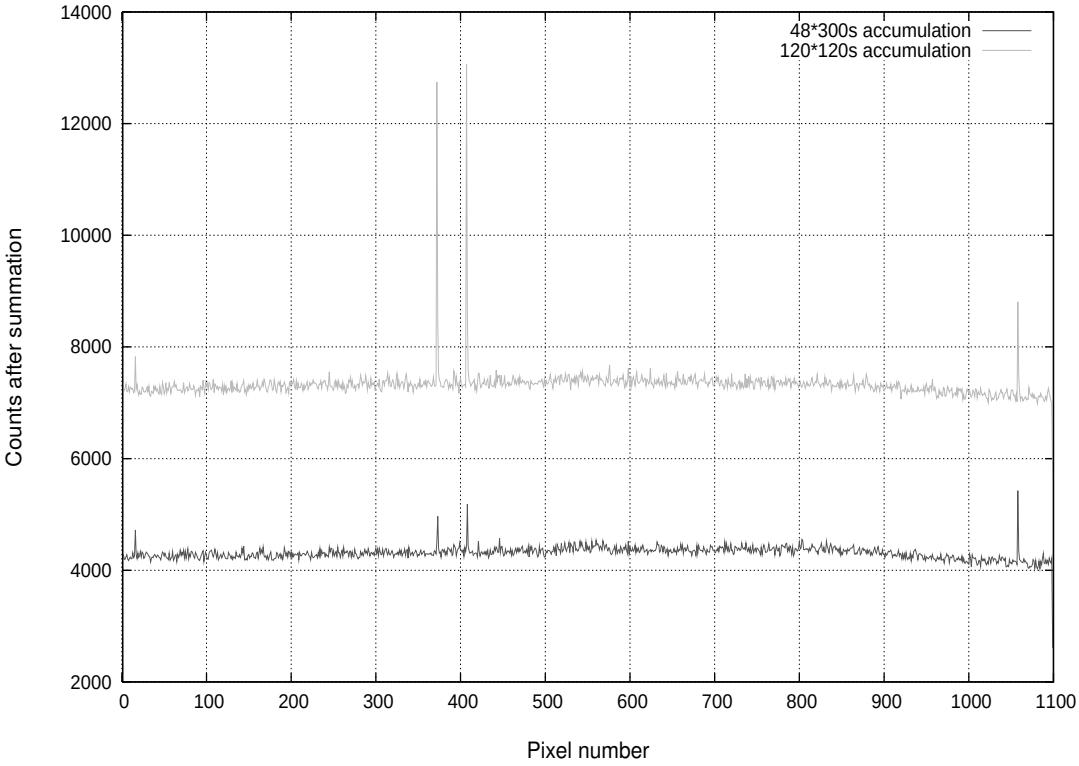

Figure A.10: Simulation - 12 axions per minute.

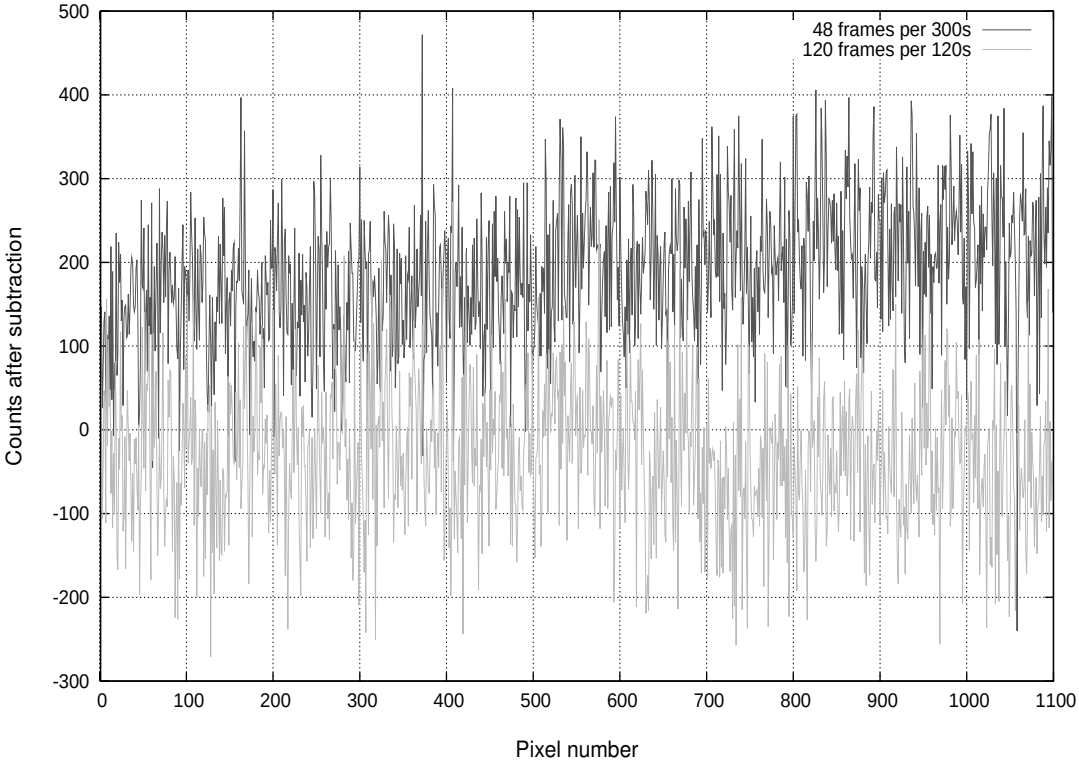

Figure A.11: Simulation - 12 axions per minute (BG subtracted).

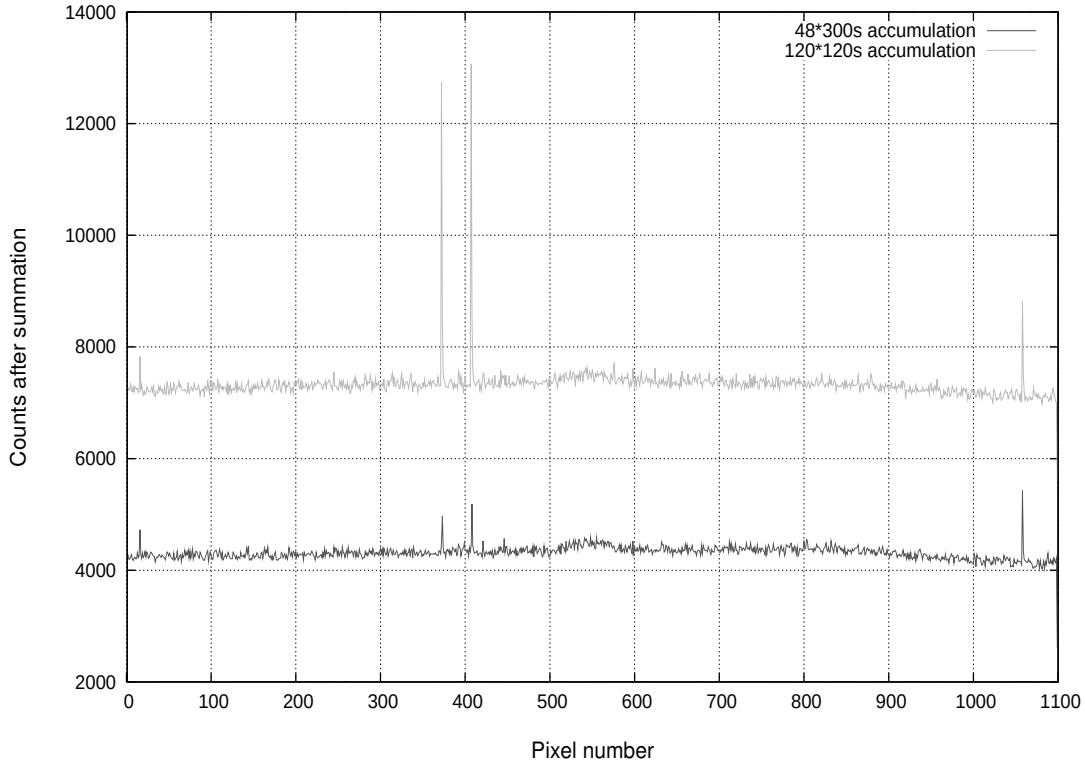

Figure A.12: Simulation - 30 axions per minute.

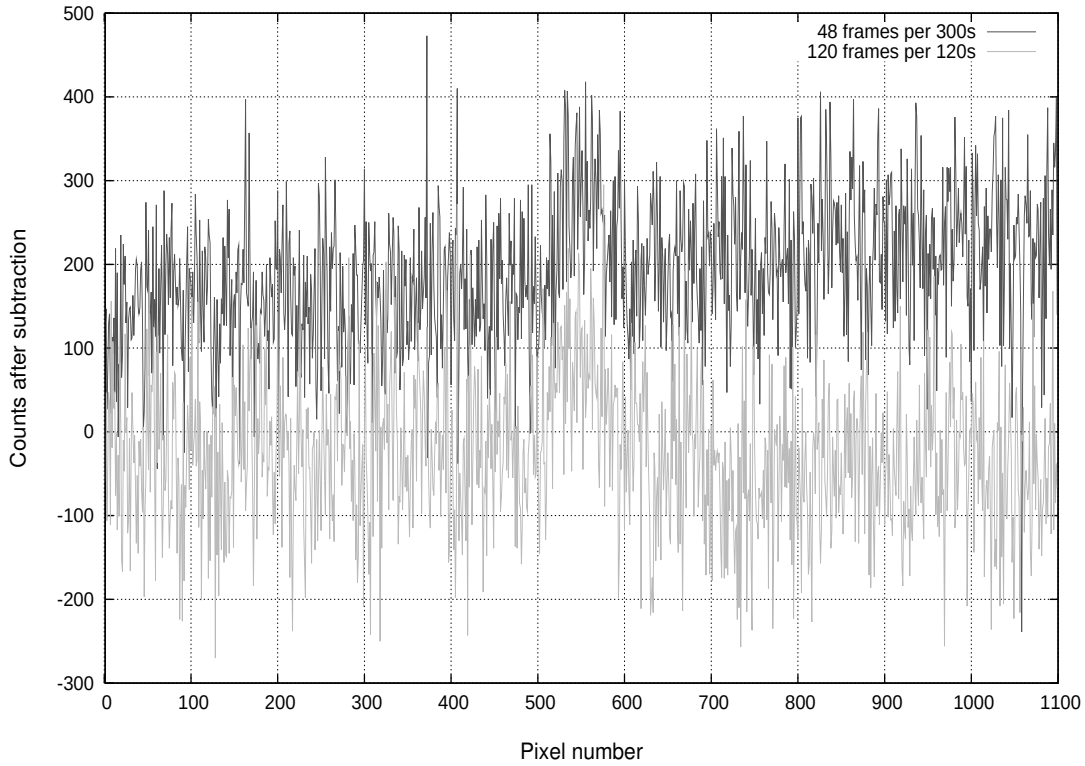

Figure A.13: Simulation - 30 axions per minute (BG subtracted).

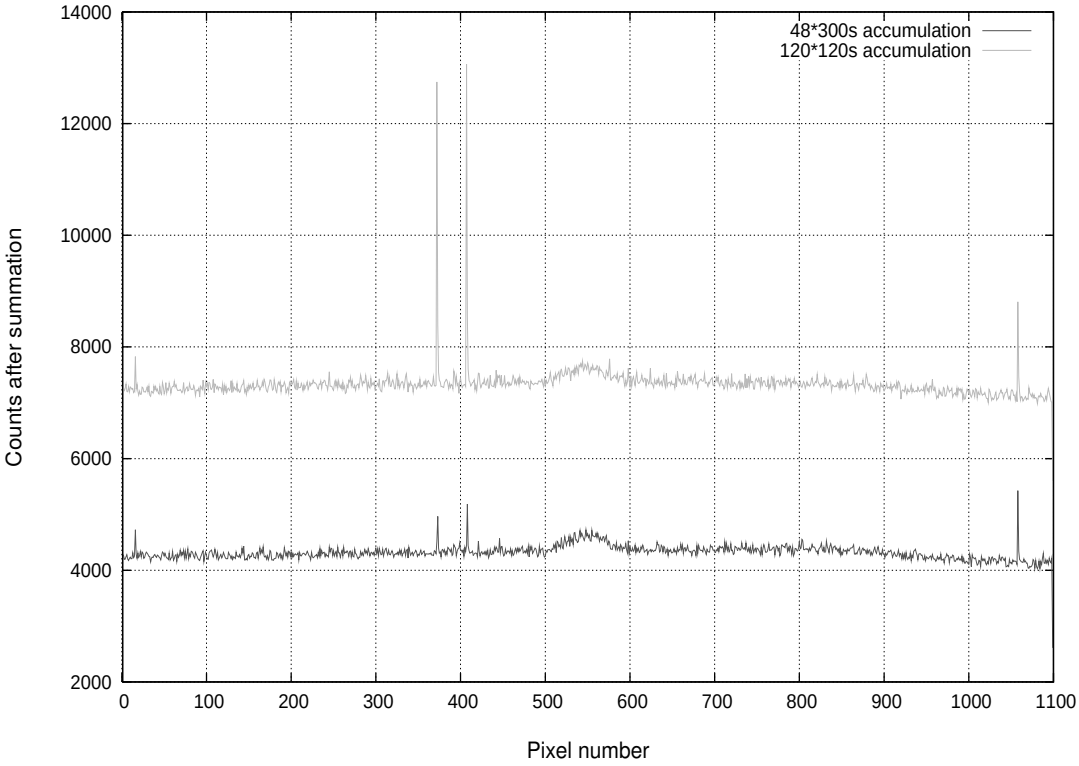

Figure A.14: Simulation - 60 axions per minute.

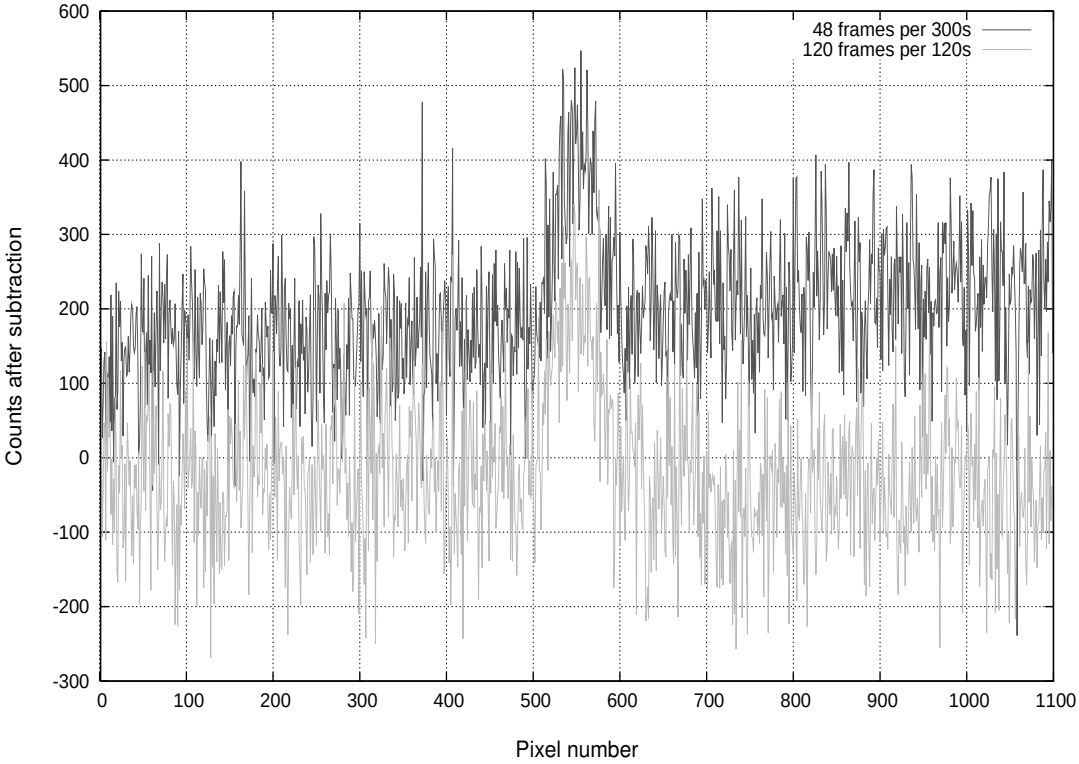

Figure A.15: Simulation - 60 axions per minute (BG subtracted).

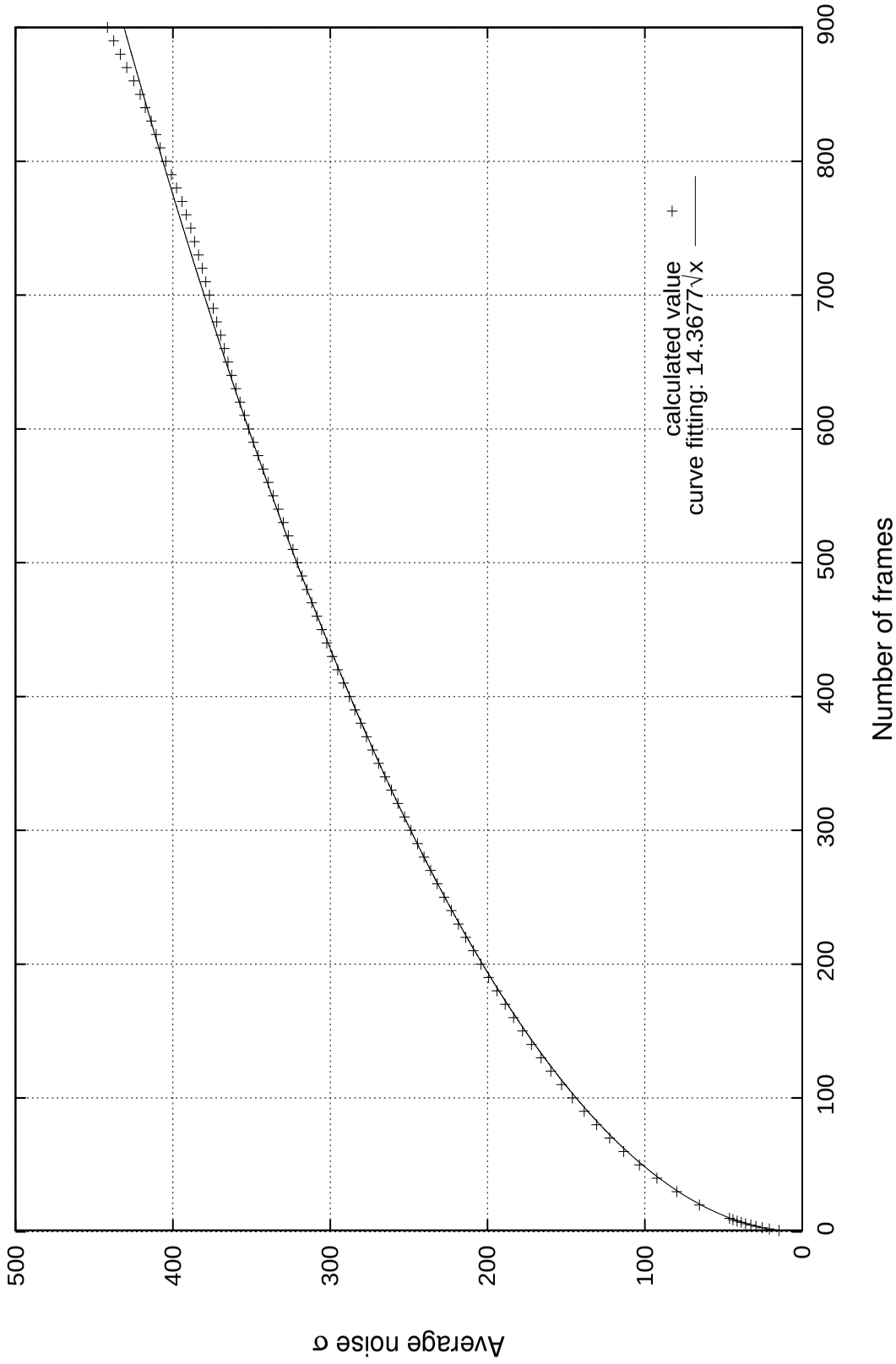

Figure A.16: Noise standard deviation development.

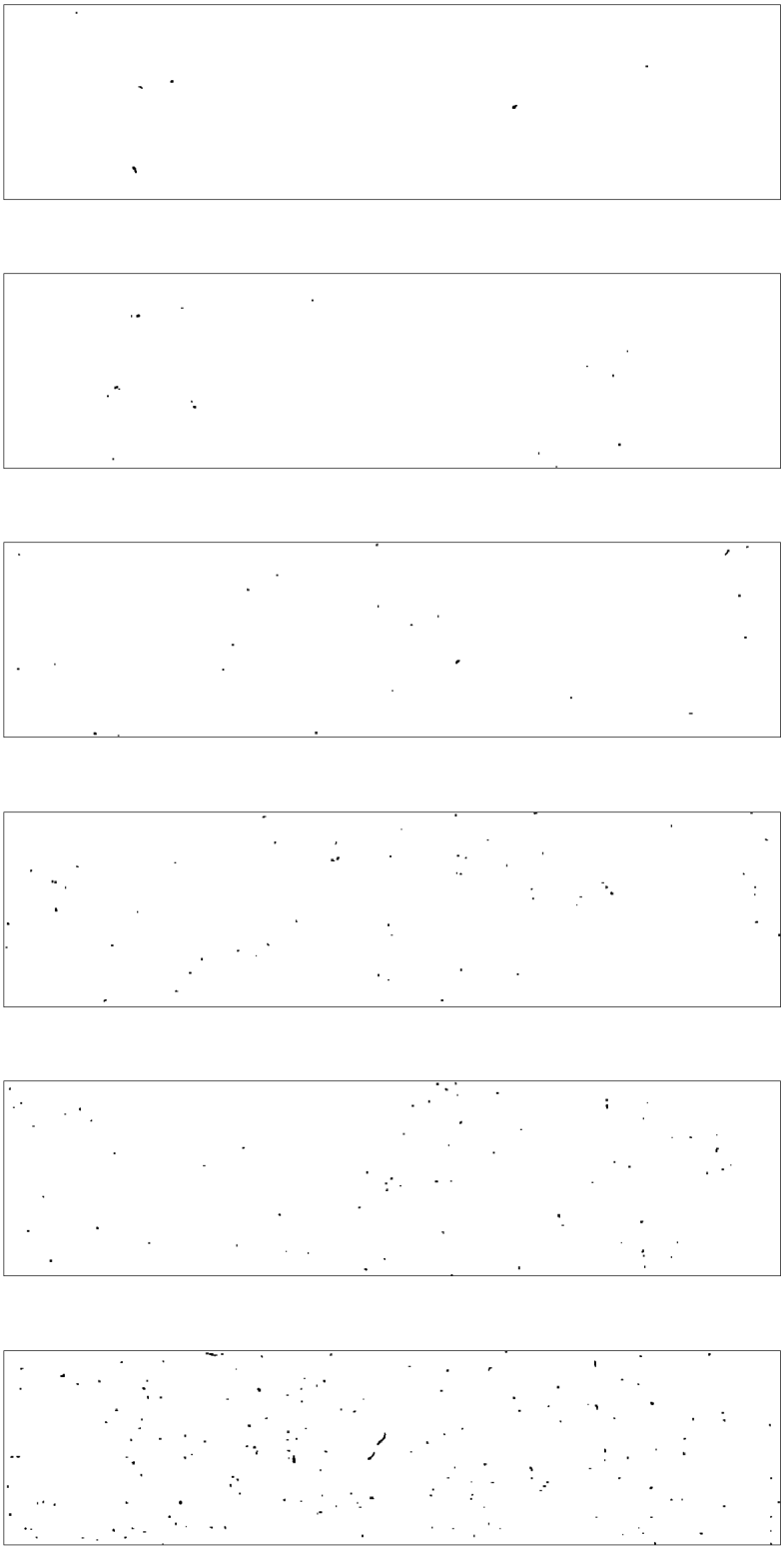

Figure A.17: Cosmic ray activity. Full frame shots with exposure times gradually increasing downwards (30s, 120s, 300s, 600s, 900s and 1800s)

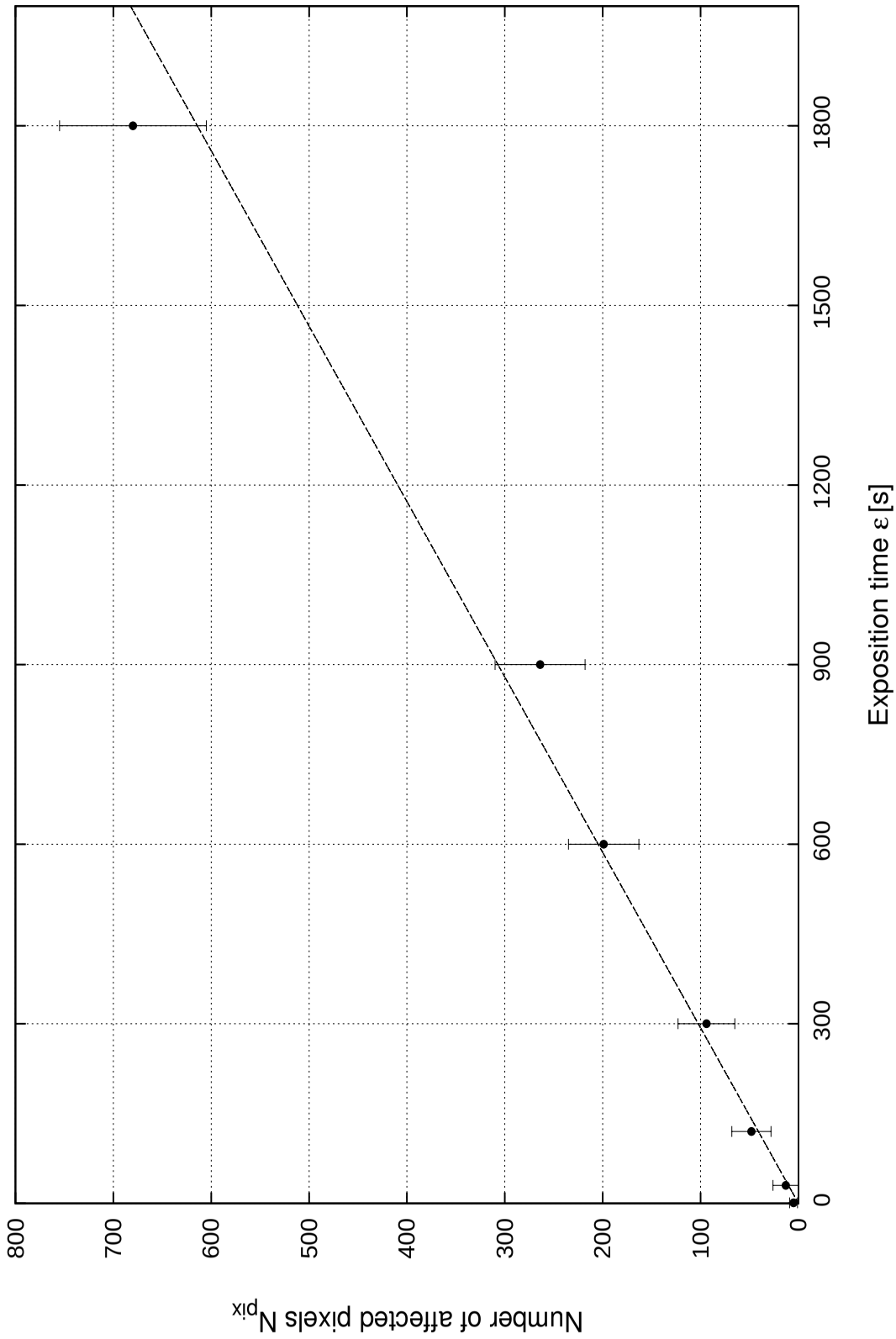

Figure A.18: Linear fit of the average number of affected pixels by the cosmic rays in respect to the exposure time.

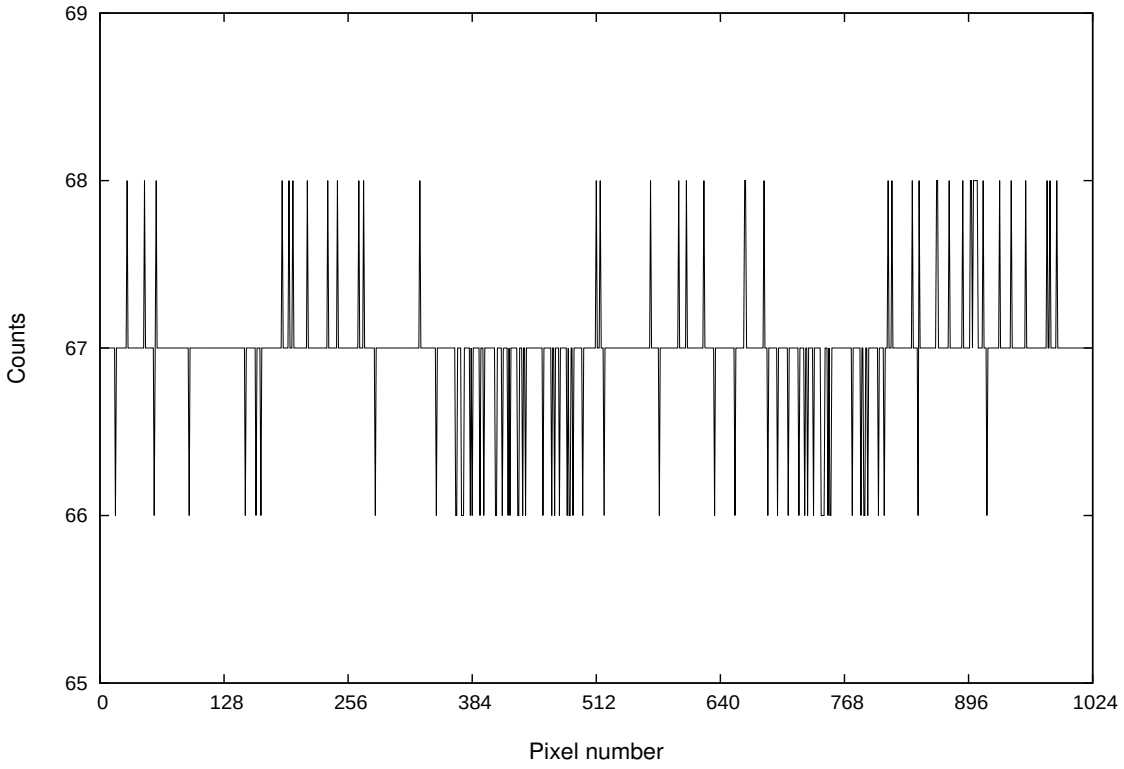

Figure A.19: Single row from a "zero" exposure time full-frame shot.

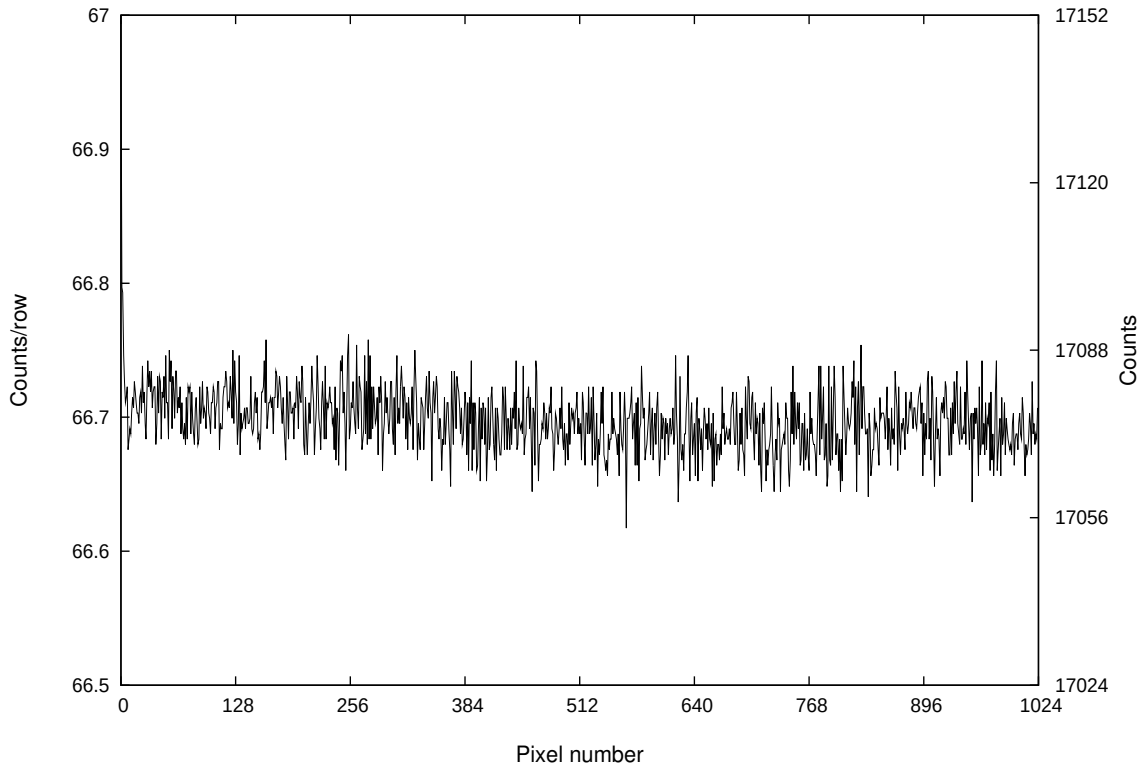

Figure A.20: Sum of the rows of the "zero" exposure time full-frame shot.

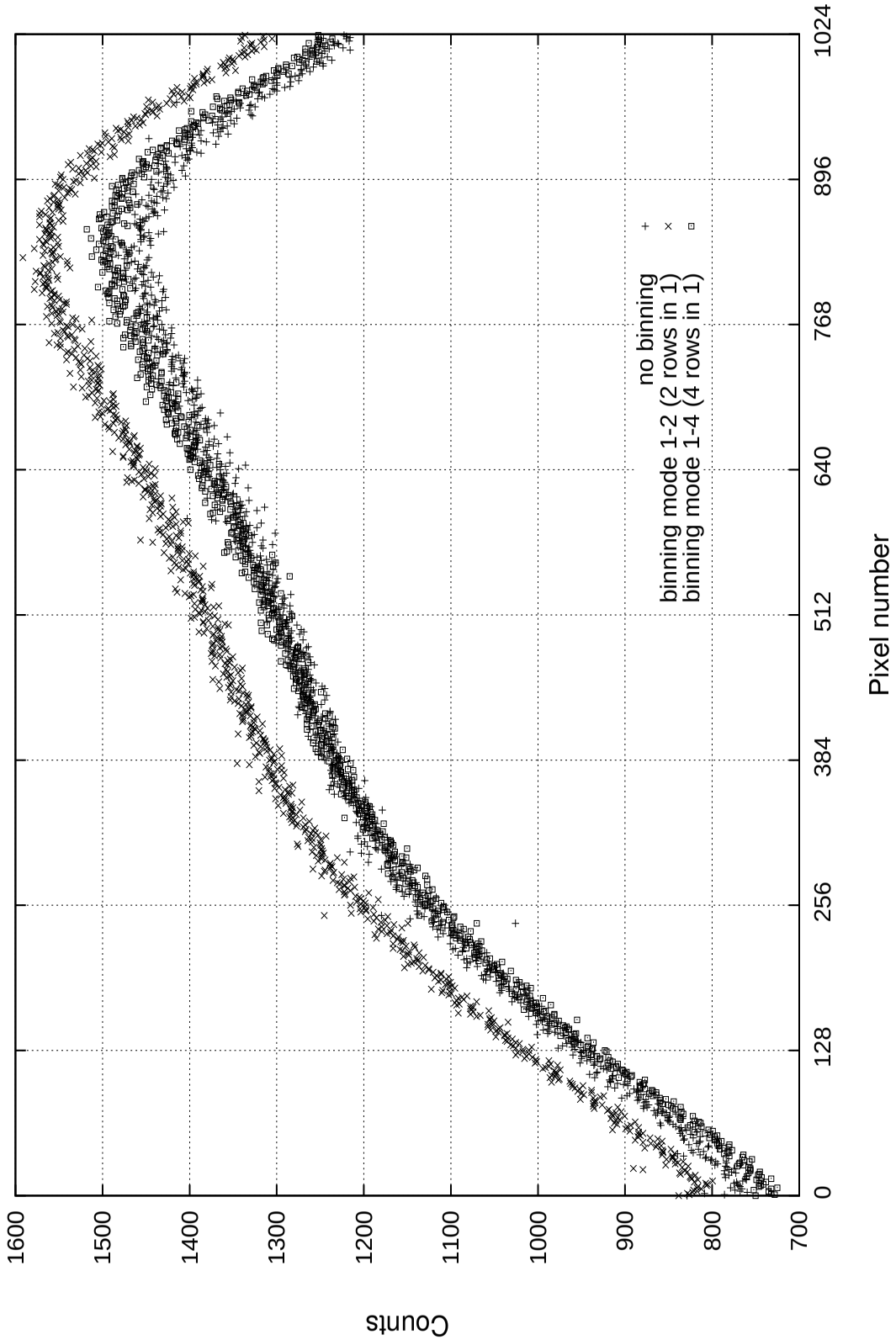

Figure A.21: Basic binning modes comparison (low light level). The highest detected total signal was obviously gained with the use of 1-2 hardware binning mode.

B Photos

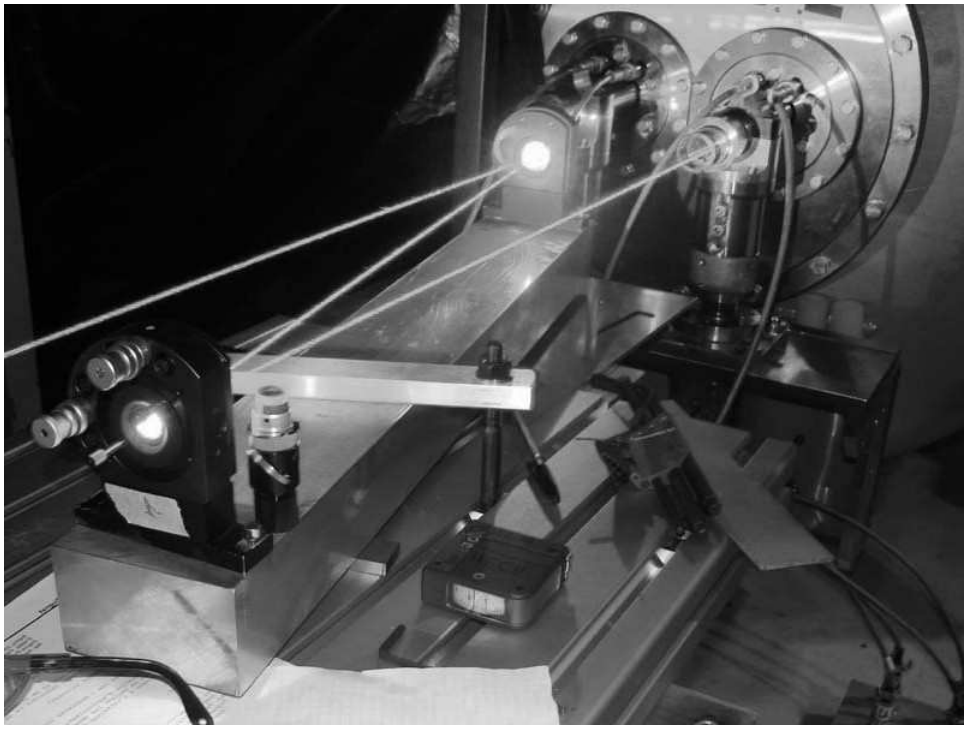

Figure B.22: Laser light at the the entrance of the first magnet of OSQAR.
source: <http://osqar.web.cern.ch/osqar/laser.jpg>

Figure B.23: Me at the detector side of OSQAR.